



National Library
of Canada

Bibliothèque nationale
du Canada

Acquisitions and
Bibliographic Services Branch

Direction des acquisitions et
des services bibliographiques

395 Wellington Street
Ottawa, Ontario
K1A 0N4

395, rue Wellington
Ottawa (Ontario)
K1A 0N4

Vous liez votre référence

Vous liez votre référence

NOTICE

AVIS

The quality of this microform is heavily dependent upon the quality of the original thesis submitted for microfilming. Every effort has been made to ensure the highest quality of reproduction possible.

La qualité de cette microforme dépend grandement de la qualité de la thèse soumise au microfilmage. Nous avons tout fait pour assurer une qualité supérieure de reproduction.

If pages are missing, contact the university which granted the degree.

S'il manque des pages, veuillez communiquer avec l'université qui a conféré le grade.

Some pages may have indistinct print especially if the original pages were typed with a poor typewriter ribbon or if the university sent us an inferior photocopy.

La qualité d'impression de certaines pages peut laisser à désirer, surtout si les pages originales ont été dactylographiées à l'aide d'un ruban usé ou si l'université nous a fait parvenir une photocopie de qualité inférieure.

Reproduction in full or in part of this microform is governed by the Canadian Copyright Act, R.S.C. 1970, c. C-30, and subsequent amendments.

La reproduction, même partielle, de cette microforme est soumise à la Loi canadienne sur le droit d'auteur, SRC 1970, c. C-30, et ses amendements subséquents.

Canada

UNIVERSITY OF ALBERTA

THE ELBOW THERMOSYPHON:

An Experimental Investigation of Its Evaporative Behaviour

by

Jialin Fu

A thesis submitted to the Faculty of Graduate Studies and Research in partial fulfilment of the requirements for the degree of Master of Science.

DEPARTMENT OF MECHANICAL ENGINEERING

Edmonton, Alberta

Fall 1993



National Library
of Canada

Acquisitions and
Bibliographic Services Branch

395 Wellington Street
Ottawa, Ontario
K1A 0N4

Bibliothèque nationale
du Canada

Direction des acquisitions et
des services bibliographiques

395, rue Wellington
Ottawa (Ontario)
K1A 0N4

Your title - Votre référence

Our title - Notre référence

The author has granted an irrevocable non-exclusive licence allowing the National Library of Canada to reproduce, loan, distribute or sell copies of his/her thesis by any means and in any form or format, making this thesis available to interested persons.

L'auteur a accordé une licence irrévocable et non exclusive permettant à la Bibliothèque nationale du Canada de reproduire, prêter, distribuer ou vendre des copies de sa thèse de quelque manière et sous quelque forme que ce soit pour mettre des exemplaires de cette thèse à la disposition des personnes intéressées.

The author retains ownership of the copyright in his/her thesis. Neither the thesis nor substantial extracts from it may be printed or otherwise reproduced without his/her permission.

L'auteur conserve la propriété du droit d'auteur qui protège sa thèse. Ni la thèse ni des extraits substantiels de celle-ci ne doivent être imprimés ou autrement reproduits sans son autorisation.

ISBN 0-315-88080-5

Canada

THE UNIVERSITY OF ALBERTA

RELEASE FORM

NAME OF AUTHOR: **Jialin Fu**

TITLE OF THESIS: **THE ELBOW THERMOSYPHON:**

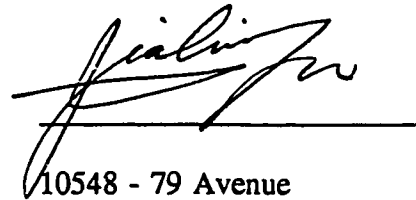
An Experimental Investigation of Its Evaporative Behaviour.

DEGREE FOR WHICH THESIS WAS PRESENTED: **Master of Science**

YEAR THIS DEGREE GRANTED: **Fall 1993**

Permission is hereby granted to **the University of Alberta Library** to reproduce single copies of this thesis and to lend or sell such copies for private, scholarly or scientific research purposes only.

The author reserves all other publication and other rights in association with the copyright in the thesis, and except as hereinbefore provided neither the thesis nor any substantial portion thereof may be printed or otherwise reproduced in any material form whatever without the author's prior written permission.



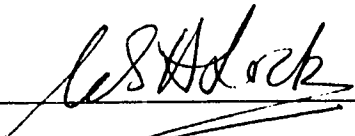
10548 - 79 Avenue

Edmonton, Alberta T6E 1R8

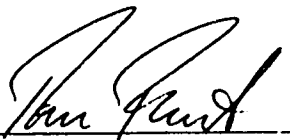
DATE: Aug. 16, 1993

THE UNIVERSITY OF ALBERTA
FACULTY OF GRADUATE STUDIES AND RESEARCH

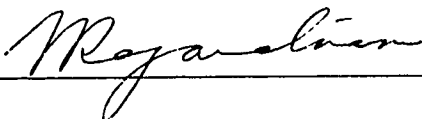
The undersigned certify that they have read, and recommend to the Faculty of Graduate Studies and Research for acceptance, a thesis entitled The Elbow Thermosyphon submitted by Jialin Fu in partial fulfilment of the requirements for the degree of Master of Science.



Dr. G. S. H. Lock (Supervisor)



Dr. T. W. Forest



Dr. N. Rajaratnam

Date August 19, 1993

To my wife, Yang.

ABSTRACT

The thesis presents the results of an experimental investigation of an evaporative, elbow thermosyphon under low pressure conditions. Emphasis is placed in three areas: firstly, the effect of filling charge on the heat transfer rate; secondly, the effect of tube geometry on the heat transfer rate; finally, the effect of tube orientation on the heat transfer performance.

Reference values of the thermosyphon parameters are chosen for comparing with the results of each test. They are: $L_H/D = L_C/D = 20$ and $v_R = 35\%$. For all the experiments, the temperature difference between evaporator and condenser is $0 < T_H - T_C < 100$ K. The experimental range of filling charge is from 10% to 75% with a fixed tube geometry. The experiments of tube geometry cover the range $10 \leq L_H/D \leq 40$ and $10 \leq L_C/D \leq 40$ while the filling charge was fixed at 35%. For the experiments on tube orientation, due to symmetry, the ranges covered are: $0 \leq \phi_l \leq \pi/2$ and $0 \leq \phi_r \leq \pi/2$ with the fixed reference values of tube geometry and filling charge.

The data reveal the hydrodynamic and thermal behaviour of the thermosyphon for a given filling charge, tube length, and inclination. Explanations of the heat transfer behaviour observed are given in each chapter. The optimum values, such as filling charge and inclination, are given for the purpose of application.

ACKNOWLEDGEMENTS

The author wishes to express his appreciation and gratitude to Dr. G. S. H. Lock for his guidance, patience, and understanding throughout the course of this work.

The author would also like to take this opportunity to thank the technicians and machinists of the Department of Mechanical Engineering, Mr. B. Ceilin and Mr. A. Muir in particular.

Financial aid from the Natural Science and Engineering Research Council of Canada under a strategic grant is greatly appreciated.

CONTENTS

Abstract

Acknowledgements

List of figures

List of tables

Nomenclature

	page
1 INTRODUCTION	1
1.1 Definition and classification	1
1.2 Application	2
1.3 Scope of thesis	5
References	10
2 PERFORMANCE OF A RIGHT-ANGLED, EVAPORATOR THERMOSYPHON	13
2.1 Introduction	13
2.2 Experiments	15
2.3 Discussion of results	17
2.3.1 Upright condenser	17
2.3.2 Upright evaporator	19
3.3 General observations	19
2.4 Conclusions	20

	page
Acknowledgements	22
References	28
3 THE INFLUENCE OF FILLING CHARGE, EVAPORATOR LENGTH AND CONDENSER LENGTH ON THE PERFORMANCE OF A RIGHT-ANGLED THERMOSYPHON	 30
3.1 Introduction	30
3.2 Experiments	32
3.3 Discussion of results	33
3.3.1 Effect of filling quantity	33
3.3.2 Effect of condenser and evaporator lengths	35
3.4 Conclusions	37
Acknowledgements	39
References	46
4 THE INFLUENCE OF EVAPORATOR AND CONDENSER INCLINATION ON THE PERFORMANCE OF A RIGHT-ANGLED THERMOSYPHON	 48
4.1 Introduction	48
4.2 Experiments	50
4.3 Discussion of results	52
4.4 Conclusions	56

	page
Acknowledgements	57
References	64
5 SUMMARY AND RECOMMENDATIONS	65
5.1 Summary	65
5.2 Recommendations for further study	66
Appendix 1 Arrangement of the experimental apparatus	67
Appendix 2 Calibration curves	70
Appendix 3 Experimental data	75
Appendix 4 Estimated uncertainty	97
Appendix 5 Empirical correlation	100
Appendix 6 Flow visualization	105

List of Figures

	page	
Fig. 1.1	Model of evaporative thermosyphon	7
Fig. 1.2	Non-linear thermosyphon configurations	8
Fig. 1.3	Model of elbow thermosyphon	9
Fig. 2.1	Schematic of elbow thermosyphon rig	23
Fig. 2.2	Heat flux density versus temperature difference for an upright condenser	24
Fig. 2.3	The effect of vapour temperature on heat transfer with an upright condenser	25
Fig. 2.4	Overall heat transfer coefficient versus temperature difference for an upright condenser	26
Fig. 2.5	Heat flux density versus temperature difference for an upright evaporator	27
Fig. 3.1	Schematic of right-angled thermosyphon	41
Fig. 3.2	Effect of filling quantity on heat transfer	42
Fig. 3.3	Effect of condenser length on heat transfer	43
Fig. 3.4	Effect of evaporator length on heat transfer	44
Fig. 3.5	Effect of length-diameter ratio on heat transfer	45
Fig. 4.1	Schematic representation inclined of right-angled thermosyphon	58
Fig. 4.2	The effect of tilt on heat transfer without rotation	59
Fig. 4.3	Effect of tilt on heat transfer with a horizontal condenser	60
Fig. 4.4	Effect of rotation on heat transfer with a horizontal evaporator	61

	page	
Fig. 4.5	Effect of tilt on heat transfer with $\phi_r = 0^\circ$	62
Fig. 4.6	Typical heat transfer contours showing the effect of tilt and rotation	63
Fig. A1.1	Arrangement of the experimental apparatus	68
Fig. A1.2	Thermocouple arrangement and location	69
Fig. A2.1	Calibration curve for $L_H/D = 10$	71
Fig. A2.2	Calibration curve for $L_H/D = 20$	72
Fig. A2.3	Calibration curve for $L_H/D = 30$	73
Fig. A2.4	Calibration curve for $L_H/D = 40$	74
Fig. A5.1	Comparison of empirical correlation with design-state results	103
Fig. A5.2	Comparison of empirical correlation with off-design-state results	104
Fig. A6.1	Schematic of flow visualization	106
Fig. A6.2	Flooding phenomenon in horizontal condenser	107
Fig. A6.3	Dry surface at the upper section of a vertical evaporator	107
Fig. A6.4	Plug flow and bubbly flow in a vertical evaporator	108
Fig. A6.5	Plug flow and bubbly flow in a tilted evaporator	108
Fig. A6.6	The weak rivulet in a tilted condenser	109
Fig. A6.7	Plug flow in the tilted evaporator	109
Fig. A6.8	Liquid slug pushed into condenser at the evaporator close to horizontal	110

List of Table

	page
Table 3.1 Test schedule	40
Table A3.1 to Table A3.42 Experimental data	76-96

Nomenclature

A	area
a	coefficient
B	coefficient
b	coefficient
c	coefficient
D	tube diameter
h	heat transfer coefficient
I	current
L	tube length
\dot{m}	mass circulation rate
Nu_D	Nusselt number based on tube diameter
P	pressure
Q	heat flux
\dot{q}	heat flux density
T	temperature
T_{ROOM}	room temperature
V	voltage
v	filling charge

Greek

λ	latent heat
-----------------------------	-------------

ε	uncertainty
Φ	dimensionless function
ϕ	angle, temperature ratio in Appendix 5
η	resistance ratio

Subscripts

A	adiabatic
C	condenser
f	reference
G	gross
H	evaporator
I	saturated
L	loss
N	net
P	pool boiling
R	ratio
r	rotation
t	tilt
1,2	heater number

CHAPTER 1

INTRODUCTION

1.1 Definition and Classification

Thermosyphons have the ability to transport very large quantities of heat with relatively small temperature differences over their working length by utilizing the buoyancy forces. An evaporative thermosyphon has a very high heat transfer efficiency normally associated with evaporation and condensation processes.

In simple form, the evaporative closed thermosyphon consists of a tube closed at both ends and containing a selected amount of working fluid usually expressed as a fraction of the tube volume. The remainder contains the vapour phase initially in equilibrium with the liquid. As indicated in Fig. 1.1, the lower section L_H locates the heat source, or evaporator, and the upper section L_C locates the heat sink, or condenser. L_A represents an adiabatic section. If the thermosyphon is placed in a gravity field, heating will cause the liquid to vaporize and rise toward to the condenser. The heat will be rejected to the environment and the condensate will return to the evaporator by gravitational force; thus the circulation will be repeated. Lock (1992) defined a thermosyphon as

any fluid system in which the prevailing temperature and

body force fields combine to produce a circulation the result of which is an enhanced thermal flux.

Thermosyphons can be classified in different ways. Davies and Morris (1965) have categorized thermosyphons depending on:

- (a) the nature of the boundaries or type of thermodynamic system -- open or closed;
- (b) the heat transfer process which takes place within the device -- natural or mixed convection (combined natural and forced convection);
- (c) the thermodynamic state of the fluid within the device -- single phase, two phase, or critical state;
- (d) the nature of the body force causing fluid circulation within the system -- gravitational or rotational.

1.2 Applications

A comprehensive literature survey of thermosyphons which fall into the previously mentioned categories has recently been carried out by Lock (1992).

Applications of the evaporative thermosyphon which have been proposed and investigated include: maintaining uniform temperatures in bakers' ovens (Moorhouse, 1960); cooling electric circuit packages (Larkin, 1973); cooling thermoelectric devices (Kolenko and Verdiev, 1973); prevention of icing on navigation buoys using the heat of the sea to de-ice the superstructure (Larkin, 1971); as pin fin elements in heat exchangers

(Larkin, 1971; Lee et al., 1978; Sakhuja, 1973); internal cooling of gas turbine blades (Cohen and Bayley, 1955; Bayley and Martin, 1971; Bayley and Bell, 1957; Edwards, 1970) and cooling electric motor rotors (Finlay, 1975). In the application of the thermosyphon to rotating systems (gas turbine blades and motor rotors), the gravitational force field is replaced by a centrifugal force field which may be in order of 10^4 g. Schmidt (1951) was the first to apply an open thermosyphon system to the gas turbine blades. Bayley and Bell (1957) reported the use of closed thermosyphons in the turbine blade cooling system. The closed thermosyphon has the advantage of fluid containment and does not have the vibrational stability problems associated with the open thermosyphon. Most researchers have stressed the importance of the closed system when dealing with gas blade cooling.

Recent developments of applications in northern nations have made the concept of thermosyphon more meaningful. Intensive reviews of the applications for thermosyphons in cold regions have been given by Lock (1992) and Cheng and Zarling (1990). They include: the maintenance of soil in a frozen and subcooled state (Long, 1963); the de-icing capability for structures, equipment and vehicles (Wilson et al., 1978; Lock, 1972; Vasiliev, 1989; Tanaka et al., 1982); the storage of food (Fukuda et al., 1990) and the storage of solar energy (Ma and Hou, 1989; Xia et al., 1990). The applications of thermosyphons in cold regions are mainly concerned with the utilization of naturally available energy sources such as ground (geothermal) energy, cold air, underground water, sea energy, hot springs, snow and ice, and solar energy.

Many of the applications mentioned above require the thermosyphon working

under different conditions, in different shapes or at different positions: single phase or two-phase; linear or non-linear; vertical, tilt, or horizontal. Fig. 1.2 illustrates the different types of non-linear thermosyphons. The fundamental principles and the physical models of them have been delineated in Lock (1992).

For a vertical, linear thermosyphon, reflux conditions take place both in the condenser and the evaporator, as shown in Fig. 1.1a. In the condenser, a wetted tube surface ensures a falling film, the thickness of which increases from the closed upper end to the lower end. At the same time, a core of vapour created by the evaporation moves upwards through a 'channel' of increasing cross-sectional area. In the evaporator, pool boiling normally exists near the lower closed end. At the upper end, a liquid film created by the returning condensate is adjacent to the wall. This situation may be affected by the tube length-diameter ratio, the filling charge and the input heat flux. The influence of those parameters on the thermal behaviour of an elbow thermosyphon will be discussed in chapter 3.

For a tilted thermosyphon, the body force field is not uniformly parallel to the tube axis. The thermal behaviour is affected by the lateral component of gravity. As shown in Fig. 1.1b, the secondary flow in the condenser section results in a film thickness which varies azimuthally, being thinnest along the upper surface of the tube and thickest along the bottom. This feature implies a radial heat flux which decreases from the upper to the lower region of the film. If the thermosyphon is close to horizontal, most of the condensate return will be contained in a thick, slowly moving rivulet which essentially converts the annular reflux pattern to a bifilamental form. In the tilted

evaporator section, the secondary circulation makes some change of bubble growth and detachment in the pool boiling region. At the upper surface of the tube, bubbles collect in greater numbers. Further away from the closed end of the evaporator, evaporation takes place in the eccentric returning condensate film.

Fig. 1.3 shows a model of an elbow thermosyphon with a horizontal condenser. In the evaporator, the situation is similar to that in the vertical, linear thermosyphon except that film beneath the inner region of the bend is thicker because more condensate return on this side. In the condenser, on the other hand, the reflux flow transforms into a bifilamental form. At the lower surface, a thick wavy rivulet moves slowly to the evaporator. Since gravity no longer acts to maintain the main circulation directly, the performance of the system is severely limited by poor drainage. If the heat transfer rate becomes too great the interaction between the vapour and the waves will produce flooding and holdup.

1.3. Scope of Thesis

A specific literature review is given in the Introduction section of each of the following chapters. As indicated, a number of investigations concerned with specific application of the evaporative closed thermosyphon can be found in the open literature. However, those concerned with basic studies of the device are few, particularly in the influence of geometry and orientation of non-linear thermosyphon on the heat transfer performance. The major objectives of this work are to explore the effects of these aspects on the heat transfer rate.

In this thesis, some preliminary experimental results of an evaporative, elbow thermosyphon will be presented in Chapter 2. Two configurations with fixed filling charge and fixed geometry are considered: a vertical condenser (with a horizontal evaporator beneath) and a vertical evaporator (with a horizontal condenser above). The influence of controlling different temperature parameters on the heat transfer rate is also indicated in the results.

Chapter 3 shifts attention to the effects of filling charge and geometry on a configuration with a horizontal condenser lying above a vertical evaporator. In the filling quantity tests, the tube length-diameter ratios, L_H/D and L_C/D , were chosen at reference values for convenience of comparing with the results in the previous chapter. Similar to the geometrical tests, the filling quantity, v_R , was fixed at 35% of the evaporator volume which was the same as that in chapter 2.

Chapter 4 is devoted to the orientation of the thermosyphon. Using the same filling quantity and evaporator and condenser lengths, a full and systematic coverage of tube inclinations has been investigated. The data reveal the complexity of hydrodynamic and thermal behaviour, as interpreted in terms of simulated flow observations. A heat flux contour map has been constructed to provide the designer with useful behavioural characteristics.

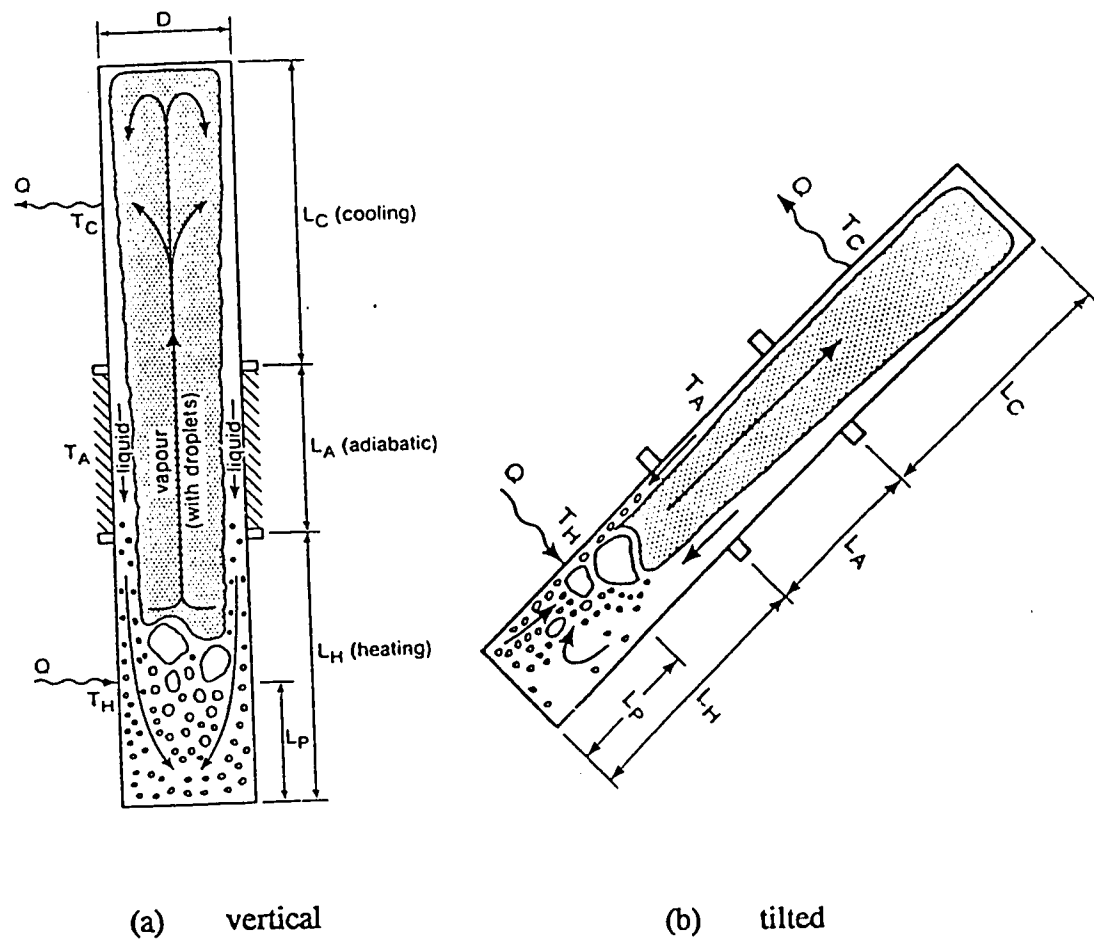
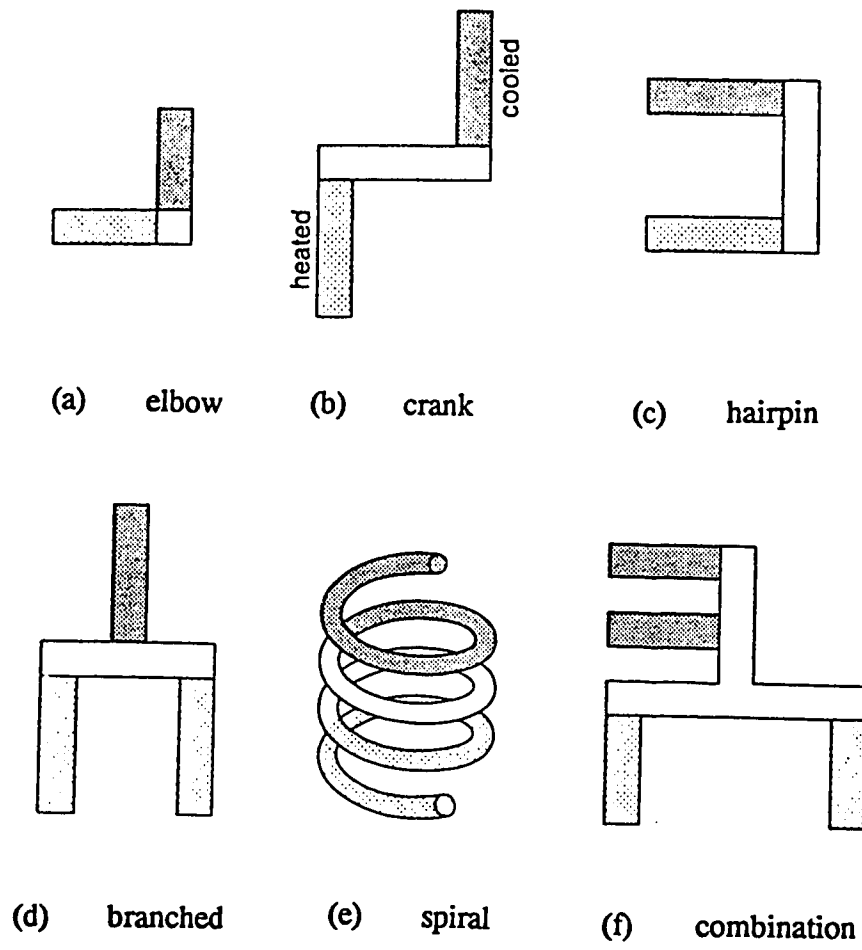


Fig. 1.1 Model of evaporative thermosyphon (after Lock 1992).



**Fig. 1.2 Non-linear thermosyphon configurations
(after Lock 1992)**

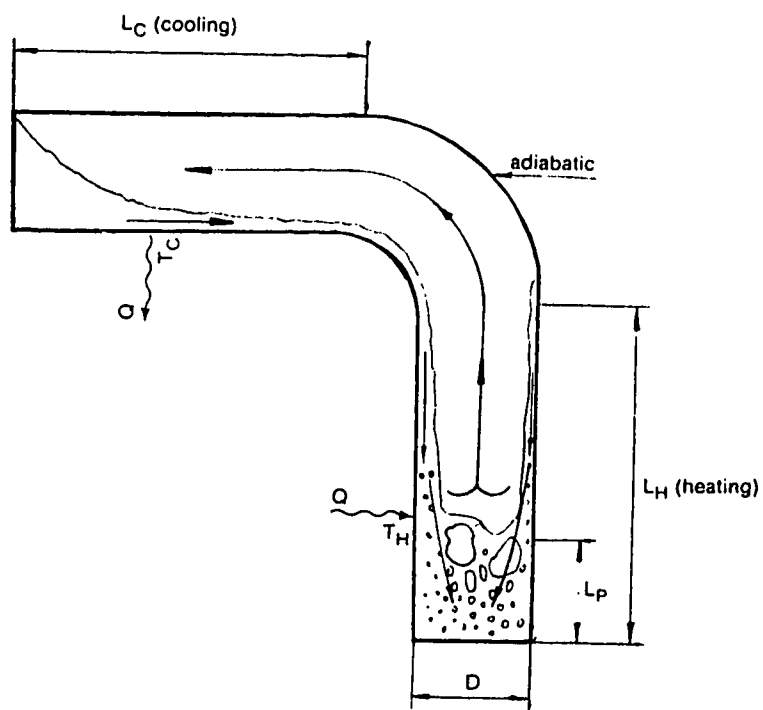


Fig. 1.3 Model of elbow thermosyphon.

References

Bayley, F.J. and Bell, N., 1957. Heat transfer characteristics of a liquid metal in the closed thermosyphon, Engineering, March.

Bayley, F.J. and Martin, B.W., 1971. A review of liquid cooling of high-temperature gas-turbine rotor blades. Proceedings of the Institution of Mechanical Engineers, 185: pp. 219-227.

Cheng, K.C. and Zarlring, J. P., 1990. Applications of heat pipes and thermosyphons in cold regions, Proc. 7th Int. Heat Pipe Conf., Minsk.

Cohen, H. and Bayley, F.J., 1955. Heat-transfer problems of liquid-cooled gas turbine blades. Proceedings of the Institution of Mechanical Engineers, 169: pp. 1063-1080.

Davies, T.H. and Morris, W.D., 1965. Thermosyphons, Engineers' Digest, Vol. 26, No. 11: pp. 87-91.

Edwards, J.P., 1970. Liquid and vapour cooling systems for gas turbines. C. P. No. 1127, Ministry of Technology, Aeronautical Research Council. London: Her Majesty's Stationary Office, 1-16.

Finlay, I.C., 1975. Heat pipes and two-phase thermosyphons. IMech. E, March: pp. 59-63.

Fukuda, M. et al., 1990. Development of an artificial permafrost storage using heat pipes. Proc. 7th Int. Heat Pipe Conf., Minsk.

Kolcnko, E.A. and Verdiev, M.G., 1973. Utilization of thermosyphon in thermoelectric devices. Geliotekhnika (Applied Solar Energy), Vol. 9, No. 1: pp.10-12.

- Larkin, B.S., 1971. An experimental study of the two phase thermosyphon tube. Transactions of the Canadian Society for Mechanical Engineering, Vol. 14, No. B-6.
- Larkin, B.S., 1973. A computer cooling application for thermosyphons. Engineering Journal, January: pp.30-33.
- Lee, Y. and Bedrossian, A., 1978. The characteristics of heat exchangers using heat pipes or thermosyphons. Int. J. Heat Mass Transfer, 21: pp.221-229.
- Lock, G.S.H., 1972. Some aspects of ice formation with special reference to the marine environment. Trans. North East Coast Inst. Eng. Shipbuild, Vol.88: pp. 175-184.
- Lock, G.S.H., 1992. The Tubular Thermosyphon. Oxford University Press, New York.
- Long, E.L., 1963. The Long thermopile. Proc. Int. Conf. on Permafrost, National Academy of Sciences, Washington, pp. 487-491.
- Ma, T., and Hou, Z., 1989. Heat pipe research and development in China. Heat Recovery Syst. CHP, 9(6): pp. 582-606.
- Moorhouse, W.E., 1960. Investigation into the reasons causing explosion in steam tubes of bakers' ovens, Proc. Inst. Mech. Eng. (London), 174(16): pp.561-574.
- Sakhuja, R.K., 1973. Flooding constraint in wickless pipes. ASME Paper No. 73-WA/HT-7.
- Schmidt, E., 1951. Heat transmission by natural convection at high centrifugal acceleration in water-cooled gas turbine blades. Paper submitted to Institute of Mechanical Engineers on Jan. 2, 1951, pp.361-363.
- Tanaka, O., Yamakage, H., Ogushi, T., Murakami, M., and Tanaka, Y., 1982. Snow

melting using heat pipes. Advances in Heat Pipe Technology. Pergamon Press, Oxford, Proc. 4th Int. Heat Pipe Conf., London 11-23.

Vasiliev, L.L., 1989. Heat pipe research and development in the USSR. Heat Recovery Syst. CHP, Vol. 9(4): pp. 313-333.

Wilson, C.H., Pope, D.H., Cundy, V.A., Nydyhl, J.E., and Pell, K.M., 1978. A demonstration project for de-icing of bridge decks. Bridge Eng., 1: pp. 189-197.

Xia, X., Wang, J.C.Y., Liu, J., and Tan, H., 1990. The heat transfer characteristics of phase change heat storage medium used in a heat pipe type solar collector. Proc. 7th Int. Heat Pipe Conf., Minsk.

CHAPTER 2

PERFORMANCE OF A RIGHT-ANGLED, EVAPORATIVE THERMOSYPHON

2.1 Introduction

In recent years, the geometry of the evaporative, tubular thermosyphon has undergone a variety of changes associated with its use in arctic engineering. representative applications include: the maintenance of frozen ground beneath engineering structures (Haynes and Zarling, 1982; Haynes et al. 1991); the de-icing of bridge decks (Wilson et al., 1978); the de-icing of railway points (Vasiliev, 1989); and the storage of foods (Fukuda et al., 1990). Many of these applications require that the thermosyphon be installed in an elbow, or right-angled, form. With the evaporator horizontal, for example, the device is suitable for ground freezing, while it lends itself to a de-icing capability when a vertical evaporator lies beneath a horizontal condenser.

Under single-phase conditions, the right-angled thermosyphon has been studied theoretically and experimentally. Lock and Park (1991) used a numerical technique to explore flow behaviour under laminar conditions, concluding that the different circulation

¹A version of this chapter has been published in *Journal of Heat Transfer*, ASME Vol. 115: pp. 501-503, 1993.

patterns in the heated and cooled sections could be reconciled by a convective coupling mechanism. Lock and Ladoon (1991), on the other hand, made observations on both laminar and turbulent behaviour in a water-filled, right-angled thermosyphon, and developed an empirical heat transfer correlation. Under evaporative conditions, the linear thermosyphon has been studied extensively. For present purposes, the nearest work is that conducted on inclined tubes (Negishi and Sawada, 1983; Terdtoon et al., 1990). In right-angled form, some empirical observations have appeared (Zarling and Haynes, 1987; Haynes et al., 1991), but there appear to have been few, if any, fundamental investigations. The purpose of this paper is therefore to provide an explanation of the heat transfer characteristics of the right-angled thermosyphon under evaporative conditions. This will consist of laboratory experiments on a small-scale apparatus using two configurations: vertical condenser (with horizontal evaporator) and horizontal condenser (with vertical evaporator).

Before describing the experiments, it is important to state the basis of the analysis. This stems from the fundamental assumption that heat flux Q is a function of the two *independent* wall temperatures T_H , T_C of the heated and cooled sections, respectively. Thus

$$Q = f(T_H, T_C) \quad (2.1)$$

or equivalently,

$$\dot{q} = g(\Delta T, T_f) \quad (2.2)$$

where $\dot{q} = Q/A_H$ is the heat flux density based on the evaporator surface area and T_f is

a convenient, but otherwise arbitrary, reference temperature such that

$$T_f = t (T_H , T_C) \quad (2.3)$$

is a single-valued function providing a second relation, which, together with ΔT , determines both T_H and T_C , and hence prescribes the heat transfer rate. $T_f = T_H, T_C$ and T_f will be used later.

2.2 Experiments

The experiments were conducted on the rig represented schematically in Fig. 2.1. This consisted of two 80 cm long copper tubes, each 2.0 cm in diameter, jointed by an elbow joint made from a tube of the same diameter. Both tube lengths were inspected for flaws but were otherwise untreated. As indicated in the figure, one length was used as the heated section, to which effect it was wrapped with heating tape, electrically insulated from the tube wall. This heating tape was installed in four 20 cm runs connected in parallel so as to permit adjustments in the local power density along the tube length. A thick layer of fibreglass insulation was then wrapped around the outside of the heater to minimize heat lost the surrounding air.

The other tube length became the cooled section. Around it were fitted four cooling jackets each covering a 20 cm run, and all being supplied with water from the building mains. This water was first directed into a distribution header where its temperature could be varied over a convenient range by varying the power supplied to a heating tape wrapped around the header outside. In this way, the cooling rate over individual 20 cm lengths of tube could be varied slightly. The elbow junction was given

a bend radius of 6 cm and was wrapped with thermal insulation during the experiments.

The power supplied to the heated section was measured in the usual way with an ammeter and voltmeter. From this gross power was subtracted the heat leakage obtained from a calibration test in which the thermosyphon was filled with thermal insulation; the power then supplied to the heater was plotted against the difference in temperature between the tube wall and the surrounding room air. Temperatures were measured throughout using copper-constantan thermocouples, the output from which via a switching box, was read on a digital multimeter. The thermocouples were located around the tube wall at intervals of 4 cm in the axial direction². One was positioned in the room air and another was installed in the tip of a 3 cm long 1 mm diameter probe inserted along the tube axis at the outer extremity of the cooled section. The latter was used to measure (saturated) vapour temperature, thus acting as a check on the vapour pressure registered by a vacuum gauge installed nearby (see Fig. A1.1).

The experimental procedure was as follows. Before the apparatus was completely assembled the inner surfaces of the tubes were cleaned using first benzene, then alcohol, and finally distilled water, the filling fluid. Assembly was then completed and the vacuum pump connected. The internal pressure was lowered toward the triple point value (near 1 kPa) and the apparatus then left for several hours with the pump switched off to ascertain that no leaks were present. At this point, a charge of water was measured and introduced using a hypodermic syringe following which the vacuum pump was again

²This description is only for the experiments in this chapter. For the other experiments in chapter 3 and 4, the thermocouples were arranged as shown in Fig. A1.2.

switched on along with the electric heater. In the presence of boiling, the remaining air was withdrawn and the tube finally sealed. Subsequently, periodic checks were made of the vapour pressure and temperature to confirm that they lay on the saturation curve.

With the apparatus thus prepared, the test runs began. Each was conducted by selecting an evaporator wall temperature T_H and then plotting the (net) heat flux density against $T_H - T_C$ for a series of condenser wall temperature T_C , noting the vapour pressure P_I at each point. Fig. 2.2 illustrates the form of the data obtained. Altering the evaporator wall temperature, the process was then repeated until the limits of the apparatus had been spanned.

2.3 Discussion of Results

In order to provide a comparison with previous work on natural convection in a right-angled thermosyphon (Lock and Ladoon, 1991), the geometry of the tube was fixed with $D = 2.0$ cm, $L_H = 40$ cm and $L_C = 40$ cm; these lengths required the use of acrylic pistons shown in Fig. 2.1. All of the runs were undertaken with water, the charge being 35% of the evaporator volume. Two configurations were tested up to the critical heat flux: a vertical condenser with a horizontal evaporator, and a horizontal condenser with a vertical evaporator.

2.3.1 Upright Condenser

With the condenser upright and the evaporator lying horizontally below, the data obtained are shown in Fig. 2.2. This displays the heat flux density \dot{q} , based on the

evaporator surface area, plotted against $T_H - T_C$ for each of a series of average evaporator wall temperatures. Cross-plotted on the same figure are curves of constant average condenser wall temperature.

The figure illustrates the general situation in which the heat flux density is a function of both T_H and T_C , not just their difference. The curves for constant evaporator temperature would be more useful in the design of an isothermal heat source, while the constant condenser temperature curves would be more appropriate to an isothermal sink; the choice thus reflects the application.

By interpolation, the above data may also be presented with the vapour temperature as a parameter. The result is shown in Fig. 2.3 which reveals the familiar performance improvement brought about by increases in vapour pressure. In this pressure range, the changes are seen to be quite small.

Fig 2.4 shows the iso- T_H data of Fig. 2.2 replotted in the form of the overall heat transfer coefficient h versus the overall temperature difference ΔT . The values of h obtained were noticeably higher than those obtained in single-phase conditions (Lock and Ladoon, 1991) but lower than those measured by Imura et al. (1979) using a vertical, linear thermosyphon. However, they were not much less than values obtained in our own apparatus when it was arranged linearly. Within experimental error, the data fit the form

$$h = a T_H - b \Delta T \quad (2.4)$$

in which a and b reflect the peculiarities of the filling fluid and chosen geometry. In view of the similarity in the individual effects of T_H , T_C , and T_I , it is to be expected that a similar form applies to the iso- T_C and T_I data.

2.3.2 Upright Evaporator

Corresponding data were also obtained with the evaporator positioned upright beneath a horizontal condenser. Fig. 2.5 shows the results plotted with the evaporator wall temperature as a parameter. These data differ from those in Fig. 2.2 in two ways. Firstly, they exhibit greater downward curvature thus making cross plots of constant T_C curves more difficult to construct; of course, it is always possible to present the data in the iso- T_C or iso- T_I forms if desired. Secondly, the data set, as a whole, lies above the upright condenser data.

2.3.3 General Observations

Both sets of data presented above are similar in form but their detailed behaviour can be quite different, not least in indicating that the upright evaporator configuration is superior to that of the upright condenser configuration. This finding is consistent with the expectation that reflux film condensation in a horizontal tube would be more efficient than in a vertical tube where the average film thickness is greater. Likewise, it is to be expected that reflux boiling in a horizontal tube would be less efficient than in a vertical tube where replacement liquid more easily covers the tube wall. However, it was surprising to find that the vertical evaporator combined with the horizontal condenser did not outperform the other configuration by much, at least for this geometry.

The limiting performance of the upright condenser configuration is typified in Fig. 2.2 by the data for $T_H = 90^\circ\text{C}$ and 95°C . Under these conditions, the local evaporator wall temperature nearer the closed end was found to rise suddenly. This indicates a

simple dryout failure caused by the inability of the returning liquid to the closed end of the evaporator.

The limiting performance with the evaporator upright is typified in Fig. 2.5 by the data with $T_H = 107$ °C. This was clearly not a simple dryout limit. It was accompanied by a periodic rise and fall in the local evaporator wall temperature near the adiabatic junction piece, thus indicating a local dryout associated with flooding and holdup in the condenser (see Fig. A6.2) while a pool continued to exist in the evaporator below. With a charge of 35% of the evaporator volume, this limit would lie well above the simple dryout limit in a vertical, linear thermosyphon, but the presence of a horizontal condenser with poor draining characteristics evidently offsets the advantage of a full evaporator.

Finally, it is worth noting that the performance of both the above configurations was beneath that obtained with the same evaporator and condenser connected in a straight line and aligned vertically. For example, with $T_H - T_C \approx 60$ K, the linear, upright evaporator and upright condenser configurations gave $\dot{q} \approx 34, 28$ and 22 kW/m², respectively. With water under single-phase conditions, the corresponding heat flux density (the same for both elbow configurations) was about 4 kW/m², confirming the anticipated thermal advantage of the evaporative system.

2.4 Conclusions

The paper presents the results of an experimental study of the right-angled, evaporative thermosyphon. Undertaken with small bore tubes, the experiments were

conducted for two configurations: an upright condenser standing above a horizontal evaporator, and an upright evaporator positioned beneath a horizontal condenser.

The data obtained with the condenser upright showed the effect of overall temperature difference on the heat flux density in tubes having the same geometry as those used previously in experiments under single-phase conditions. As expected, the performance of the evaporative system was found to be superior to that of the non-evaporator system. The parametric role of the evaporator wall temperature, the condenser wall temperature and vapour saturation temperature was demonstrated, each revealing a monotonic effect.

With the evaporator upright, the data were found to be similar and were displaced upwards relative to the upright condenser data. The upright evaporator thus gave the better performance, but not overwhelmingly so. The limit of performance with the condenser upright was found to be dictated by evaporator dryout, while that in the upright evaporator configuration corresponded to flooding in the poorly draining condenser.

For the geometry considered, both configurations of the evaporative, right-angled thermosyphon were found to be inferior to the linear, evaporator system, aligned vertically, but both were much superior to the single-phase, right-angled thermosyphon.

Acknowledgements

This work was undertaken under the auspices of the Natural Science and Engineering Research Council of Canada to whom we are grateful. We would also like to thank the technicians and machinists of the Department of Mechanical Engineering, Mr. B. Ceilin and Mr. A. Muir in particular.

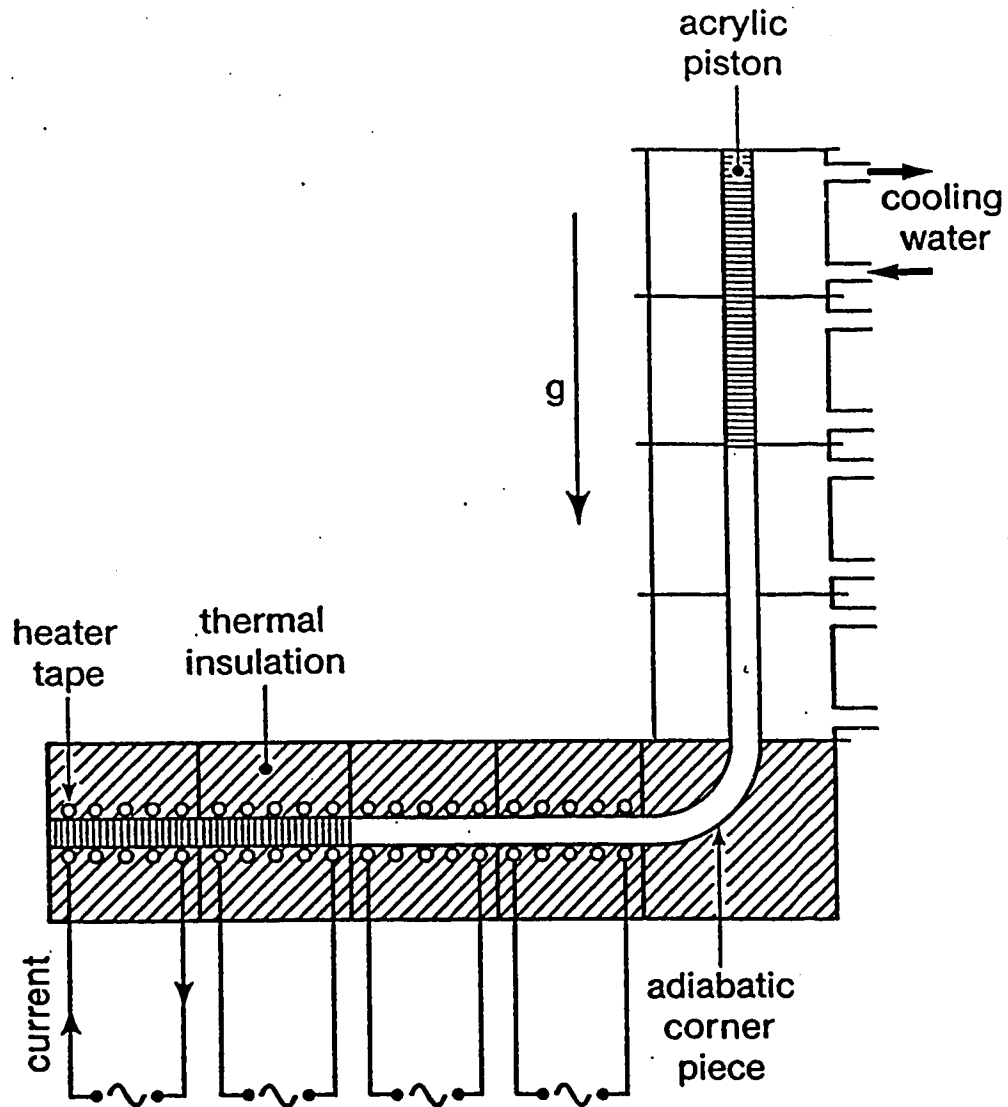


Fig. 2.1 Schematic of elbow thermosyphon rig.

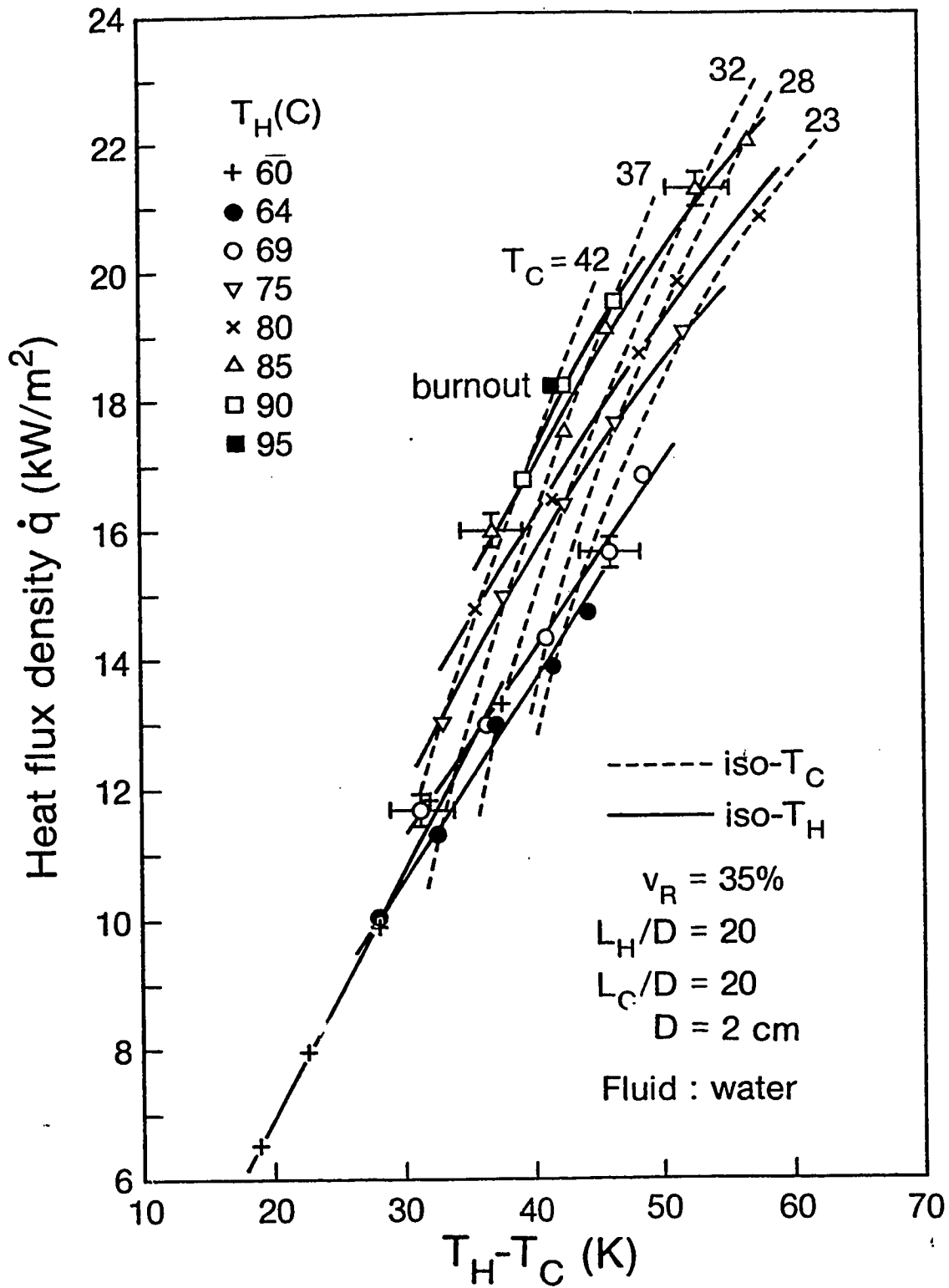


Fig. 2.2 Heat flux density versus temperature difference for an upright condenser.

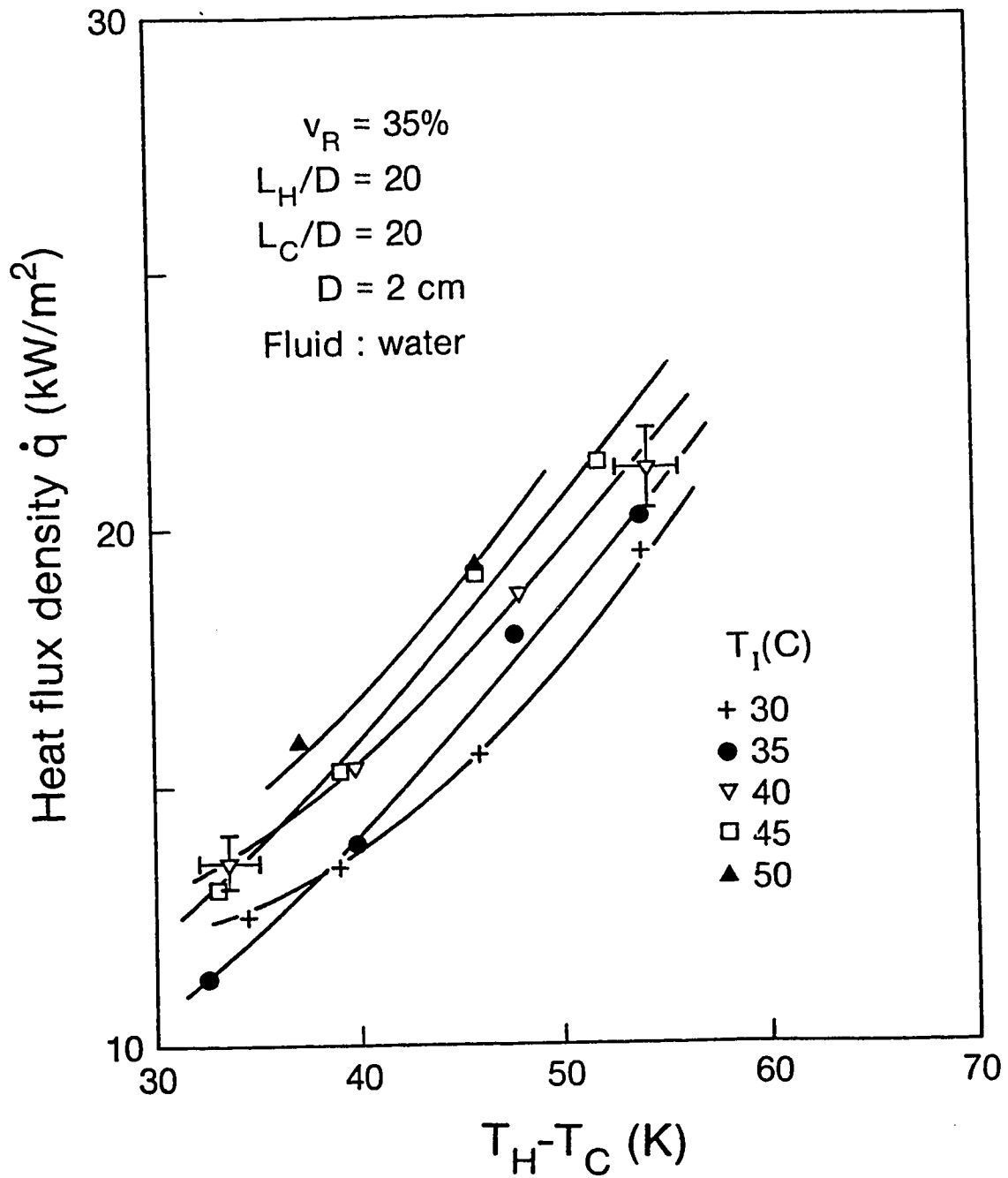


Fig. 2.3 The effect of vapour temperature on heat transfer with an upright condenser.

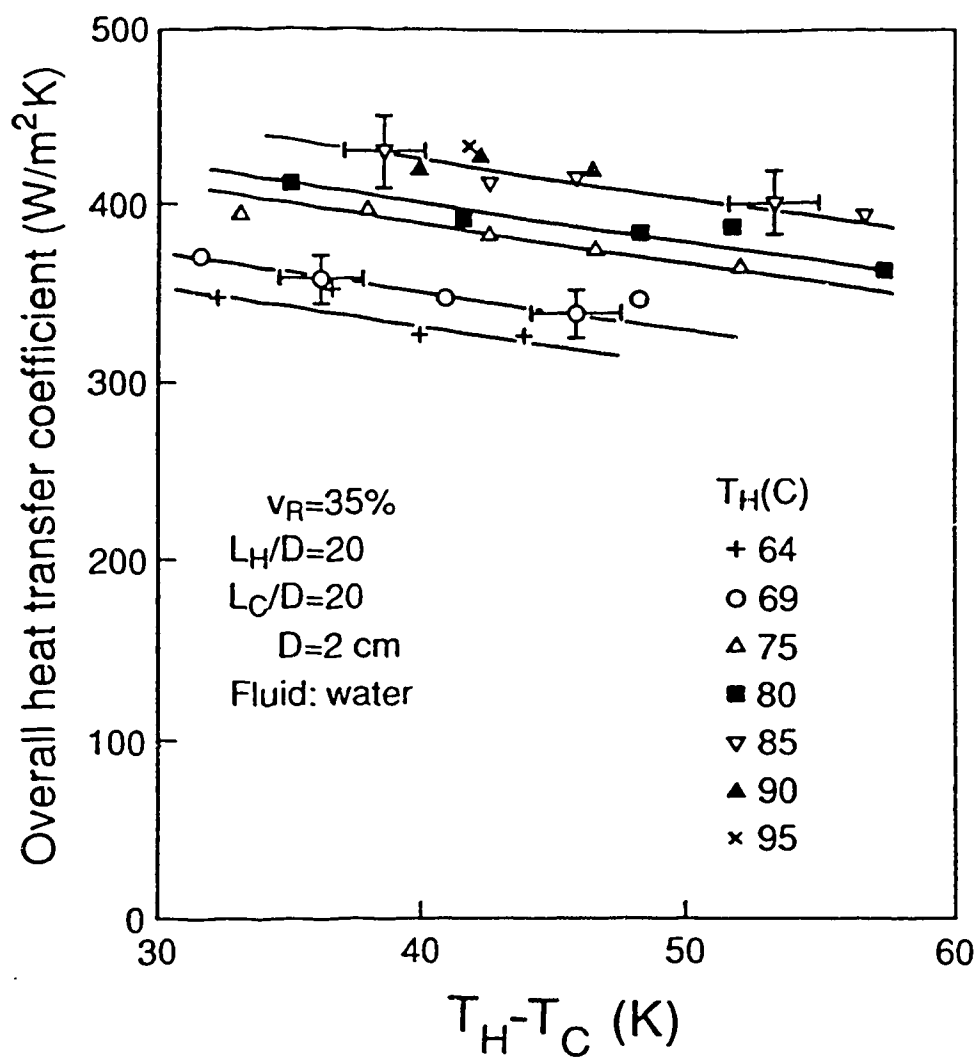


Fig. 2.4 Overall heat transfer coefficient versus temperature difference for an upright condenser.

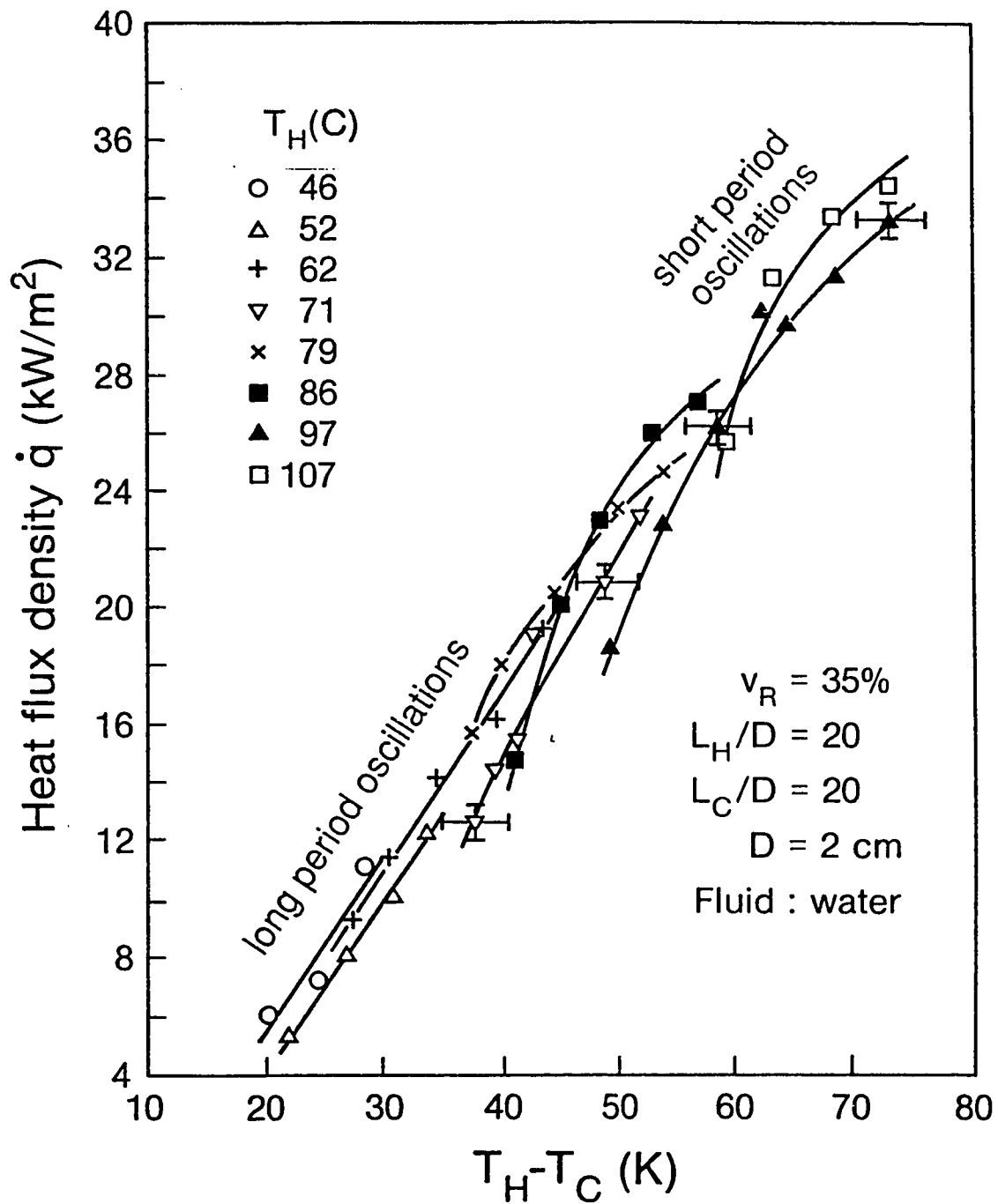


Fig. 2.5 Heat flux density versus temperature difference for an upright evaporator.

References

- Haynes, F.D. and Zarling, J.P., 1982, A comparative study of thermosyphons used for freezing soil, ASME Paper #82-WA/HT-40.
- Haynes, F.D. Zarling, J.P. Quinn, W.F. and Gooch, G.W., 1991, Laboratory tests with a hybrid thermosyphon, Proc. 10th Int. Conf. on Offshore Mech. and Arctic Eng., ASME IV: pp. 93-100.
- Imura, H. et al., 1979, Heat transfer in two-phase closed type thermosyphon, Heat Transfer--Japanese Research, Vol. 8(2): pp. 41-53.
- Lock, G.S.H. and Ladoon, D., 1991, Heat transfer in a right-angled thermosyphon, Proc. 10th Int. Conf. on Offshore Mech. and Arctic Eng., ASME IV: pp. 261-266.
- Lock, G.S.H. and Park, S., 1991, A numerical study of the right-angled thermosyphon, Proc. 10th Int. Conf. on Offshore Mech. and Arctic Eng., ASME IV: pp. 113-118.
- Negishi, K. and Sawada, T., 1983, Heat transfer performance of an inclined, two-phase, closed thermosyphon, Int. J. Heat Mass Transf., Vol. 26(2): pp. 1207-1213.
- Terdtoon, P. Shiraishi, M. and Murakami, M., 1990, Investigation of effect of inclination angle on heat transfer characteristics of closed two-phase thermosyphon, Proc. 6th Int. Heat Pipe Conf., Minsk B9P.
- Fukuda, M. Tsuchiya, F. Ryokai, K. Mochizuki, M. and Mashiko, K., 1990,

Development of an artificial permafrost storage using heat pipe, Proc. 7th Int. Heat Pipe Conf., Minsk.

Vasiliev, L.L., 1989, Heat pipe research and development in the USSR, Heat Recovery Systems and CHP., 9(4): pp. 313-333.

Wilson, C.H. Pope, D.H. Cundy, V.A. Nydahl, J.E. and Pell, K.M., 1978, A demonstration project for de-icing of bridge decks, Bridge Engineering, 1: pp. 189-197.

Zarling, J.P. and Haynes, F.D., 1987, Heat transfer characteristics of a commercial thermosyphon with an inclined evaporator section, Proc. 6th Int. Offshore Mechanics and Arctic Engineering Symposium IV: pp. 79-84.

CHAPTER 3

³THE INFLUENCE OF FILLING CHARGE, EVAPORATOR LENGTH AND CONDENSER LENGTH ON THE PERFORMANCE OF A RIGHT-ANGLED THERMOSYPHON

3.1. Introduction

In the first half of this century, the use of the evaporative thermosyphon as a device for creating and maintaining frozen ground was unknown. The first suggestion appears to have been made by Long (1963). Since then the device has found numerous northern geotechnical applications, principally in construction where the structural integrity of soil must be preserved during the summer period. Evaporative thermosyphons have thus been used to combat thaw effects through latent heat storage built up in the soil under cold, winter conditions.

In recent years, the range of geotechnical applications has expanded considerably in response to changing architectural, economic and environmental demands (Haynes and Zarling, 1988). At the same time, entirely new uses have been proposed (Lock, 1992).

³A version of this chapter has been published in the Proceedings of the 12th International Conference on Offshore Mechanics and Arctic Engineering, Vol. IV: pp. 207-211, Glasgow, 1993.

Principally among the latter is the long standing need to provide an anti-icing or de-icing capability for structures, equipment and vehicles which must operate in an atmosphere where cold winds combine with water to create large amounts of surface ice. Examples include the following: the de-icing of bridge decks (Wilson et al., 1978); the de-icing of railway points (Vasiliev, 1989); the de-icing of pavements (Tanaka et al., 1982); and the de-icing of shipboard surfaces (Lock, 1972).

Many of the above applications call for a design in which the thermosyphon tube can no longer remain straight. In particular, it is common to find situations in which a vertical evaporator stands upright beneath a horizontal condenser; for example, when the iced surface is part of a deck or paved surface. This right-angled configuration, shown schematically in Fig. 3.1, is the subject of this paper. It has been studied briefly in a previous paper (Lock and Fu, 1992) from which several conclusions were drawn. Firstly, the choice of a suitable temperature parameter in a complete thermal description is largely a matter of convenience. Secondly, the vertical evaporator configuration was slightly better than the vertical condenser configuration from a heat transfer standpoint. Thirdly, both configurations performed slightly worse than the corresponding linear tube aligned vertically.

The present work extends the earlier, exploratory study in two ways: firstly, by removing the restriction on the filling quantity v_R which was fixed at 35% of the evaporator volume; secondly, by relaxing the geometrical restriction which was fixed by $L_H/D = L_C/D = 20:1$. The paper is thus an experimental investigation of a right-angled, evaporative thermosyphon with special reference to the effect of charge and geometry on

heat transfer performance when the condenser lies horizontally above the vertical evaporator.

3.2. Experiments

The apparatus has been fully described in the earlier paper (Lock and Fu, 1992) and will not be discussed in detail here. It is sufficient to note that it consisted of a small bore (2 cm dia.) copper tube heated electrically in 20 cm lengths, and cooled with a water jacket, also in 20 cm lengths (see Fig.A1.1). In any test, the heat loss, obtained from a calibration curve, was subtracted from the gross power supplied electrically to determine the net rate of heat transfer through the system.

Temperatures were measured throughout with copper-constantan thermocouples located at 5.5 cm intervals along the tube walls and in the room air (see Fig.A1.2).

The test procedure was as follows. Firstly, the tubes were cleaned using benzene, alcohol and distilled water, in that order. A vacuum pump was then connected to the apparatus and the air pressure lowered toward the triple point pressure (≈ 1 kPa). After a period of several hours, allowed to ascertain that no leaks existed, a charge of water was introduced using a hypodermic syringe. The electric heater was then switched on followed by the vacuum pump. This permitted the remaining air (and some water vapour) to be purged while the water boiled gently. The apparatus was then sealed. Periodic measurements were subsequently made to ensure that the vapour pressure and temperature lay on the saturation curve.

The tests were then begun. These consisted of plotting the heat flux density \dot{q}

(based on the heated surface area) versus the temperature difference between the evaporator tube wall T_H and the condenser tube wall T_C . Each of these wall temperatures was calculated as the (spatial) average of at least twenty readings distributed over the tube length. With the \dot{q} versus $(T_H - T_C)$ curve completed the procedure was then repeated after changing one of the following: filling charge, condenser length or evaporator length. The test schedule is shown in Table 3.1. All tests were conducted with water as the working fluid. While it is recognized that water could not be used in a low temperature application, the behaviour under study is representative of any fluid, including many refrigerants, which operates closer to its triple point than its critical point. To simulate this behaviour a simple set of auxiliary experiments was undertaken using air bubbling into water inside a right angled, transparent tube having the same dimensions. Since

$$\dot{q} A_H \approx \dot{m} \lambda \quad (3.1)$$

where A_H is the evaporator tube surface on which the heat flux density \dot{q} is based, the corresponding mass flow rate \dot{m} in the simulated isothermal experiment could be calculated and set by adjusting and matching the upward air bubbling rate to the downward water flow rate.

3.3 Discussion of Results

3.3.1 Effect of Filling Quantity

Using the reference geometry (Test #1) the effect of filling quantity is displayed in Fig. 3.2. As indicated, the filling quantity v_R , expressed as a fraction of the

evaporator volume, extends over the range $10\% < v_R < 75\%$. The data suggest three behavioural régimes: low filling ($v_R \leq 25\%$), intermediate filling ($25\% \leq v_R \leq 50\%$) and high filling ($v_R \geq 50\%$).

Under low filling conditions it is evident that the heat transfer rate is also low, e.g. $\dot{q} \leq 5 \text{ kW/m}^2$. While this heat flux density is much higher than a typical value for single-phase conditions (Lock and Ladoon, 1991), it reveals a severe limit on evaporative performance. Since a low filling quantity compromises the ability of the liquid to cover the entire surface of the tube wall, it is to be expected that its effect in the condenser would differ from that in the evaporator. In the condenser, a thin film would tend to promote heat transfer. In the evaporator, on the other hand, if the film becomes too thin it will break, under the influence of a Weberian instability, into a set of rivulets. Between the rivulets, the tube wall is bare, thus giving rise to local overheating attributable to inefficient conduction. The overall conductance in the evaporator must then combine the effects of evaporation from the rivulets with conduction into vapour. This type of behaviour has been reported by Negishi and Sawada (1983) using very small filling quantities in inclined tubes. It appears to explain the poor overall performance of the system when v_R is small.

For intermediate filling quantities, it is to be expected that conditions in the evaporator and condenser would both change. A thicker film appears in the condenser, increasing thermal resistance, but its overall effect is evidently small in comparison with the improvement produced in the evaporator. No longer are bare patches of any extent likely to be found on the evaporator wall. Thin film evaporation in the upper reaches of

the evaporator is then combined with boiling in the liquid pool below. The net effect is to decrease the overall thermal resistance of the system, as indicated in Fig. 3.2.

For higher filling quantities, the situation changes yet again. As v_R increases, the liquid pool depth also increases, thus extending the region of pool boiling but reducing the region in which film evaporation occurs. The net effect on the evaporator appears to be negligible perhaps because bubbly flow is partially replaced by churn flow. At the same time, however, the phase change is more likely to expel liquid slugs into the condenser thus reducing its performance. Fig. 3.2 suggests that these effects combine to produce a slight deterioration in overall heat transfer rate, a situation which would presumably worsen if v_R were increased further. It thus appears that an optimum value of v_R exists. In these experiments, this value lay in the range $35\% < v_R < 50\%$. The data of Negishi and Sawada (1983) reveal a shallow optimum for ethanol but not for water.

3.3.2 Effect of Condenser and Evaporator Lengths

The effect of changing a tube length is to alter two independent geometrical ratios: the length-diameter ratio of the tube L/D , and the length ratio between the tubes L_H/L_C . This second effect may be studied in various ways. Here it was done by varying one tube length while the other was fixed at the reference value ($L/D = 20$). As Table 3.1 indicates, this enables L_H/L_C to be varied in the practical range $0.5 < L_H/L_C < 2.0$. The results are shown in Figs. 3.3 and 3.4 with the reference filling quantity of $v_R = 35\%$.

Fig. 3.3 reveals that the effect of changing the condenser length was quite small, even though the resistance ratio $\eta = (T_I - T_C)/(T_H - T_I)$ was of order 1.0. Changes in condenser resistance evidently play only a minor role. Small effects are evident at both low and high heat flux densities. For low values of q , the larger surface area of the condenser for $L_C/D = 40$ evidently creates a thinner, slower-moving film with a correspondingly higher heat transfer rate; no such advantage accrues with the thicker, faster moving film associated with $L_C/D = 10$. At higher heat fluxes, the impeding effect of the returning vapour on the rivulet draining along the bottom of the condenser creates a small deterioration, the effect being more noticeable on the shorter condenser tube, as expected.

Fig. 3.4 reveals that the evaporator plays a more crucial role in determining overall behaviour. This is especially evident in the data for $L_H/D = 10$. By comparison with the low v_R data in Fig. 3.2 such low heat transfer rates are reminiscent of a dryout condition. However, they cannot be explained by a simple dryout because pool boiling was identified in the bottom of the evaporator. The explanation appears to be as follows. As L_H/D decreases, evaporation eventually approaches the classical limit of pure pool boiling on which the tube geometry has little influence. Individual vapour bubbles then burst on, or immediately above, the free liquid surface and create only a minor splashing effect on the tube wall above. The limited vapour thus produced presents a high thermal resistance in the section of tube above the pool (Fig. A6.3). Heat transfer and evaporation rates are therefore reduced. The thin film returning from the condenser is largely evaporated in the upper reaches of the evaporator tube thereby maintaining bare patches above the pool.

This type of behaviour evidently persists until the height of the pool is great enough to permit significant bubble coalescence. That is, once vapour bubble diameters approach the tube diameter, hydrodynamic behaviour alters dramatically. At the very least, vapour slugs create thin liquid layers adjacent to the tube wall thus enhancing the heat transfer rate (see Fig. A6.4). Fig. 3.4 suggests that this transition occurred with $10 < L_H/D < 20$. The effect of large vapour bubbles evidently continues to increase as L_H/D is increased further.

Similar observations apply to Fig. 3.5 which shows the effect of changing the overall length-diameter ratio of the thermosyphon; that is, altering L_H/D and L_C/D while maintaining $L_H/L_C = 1.0$. Keeping in mind that the condenser thermal resistance is the lower, the low data points may again be attributed to dryout above the pool in the evaporator. Likewise, the monotonic increase in heat transfer rate with increased L/D again reveals a gradual shift in two-phase flow dynamics. It is not known if the highest heat transfer rates correspond to a plug flow or reflect a breakthrough into an annular régime in which a vapour core is finally established within a continuous condensate film.

3.4 Conclusions

The paper reports an experimental investigation of a small-bore, right-angled, thermosyphon under evaporative conditions. In an attempt to extend previous work to cover the effect of filling charge and tube geometry on heat transfer performance, a number of observations were made. From these, several conclusions may be drawn and applied to evaporative behaviour in fluids well below their critical point.

The effect of filling quantity, as measured by v_R , the percentage of the evaporator

volume occupied by the liquid, divided naturally into three behavioural régimes. For low charges, it is suggested that low heat transfer rates are caused by simple dryout; no pool exists at the bottom of the evaporator. For high charges, it is suggested that liquid expulsion into the condenser causes a deterioration in performance. Between these régimes is a third "optimal" régime in which liquid covers the entire wall of the evaporator.

The effect of tube geometry was explored by varying the condenser and evaporator lengths separately and together. The independent effect of condenser length was found to be small. The independent effect of evaporator length, on the other hand, was much greater. This has been attributed to the changing hydrodynamic behaviour of the bubbles created in the basal pool. It is suggested that as their effective diameter approaches the tube diameter, as the result of coalescence, they create conditions ranging from bubbly flow (for smaller length-diameter ratios) to plug flow (for larger length-diameter ratios). This gradual increase in void fraction, accompanied by a fully-wetted evaporator wall, is evidently the cause of increased evaporation and heat transfer rates.

From the standpoint of the designer, the above observations draw attention to two important considerations. Firstly, the filling quantity must be great enough to avoid simple dryout at the bottom of the evaporator; this is easy to prescribe. Secondly, low pressure behaviour can be used to advantage by ensuring an evaporator tube length great enough to shift hydrodynamic behaviour beyond the bubbly régime; this is easily done with small bore tubes but may be more difficult to prescribe with bores too large to facilitate coalescence.

Acknowledgements

This work was funded by the Natural Sciences and Engineering Research Council of Canada to whom we are indebted. We also wish to thank Brian Ceilin and Allan Muir for their help with the apparatus.

Test Number	L_H/D	L_C/D	$v_R\%$
1	20	20	35
2	20	20	10
3	20	20	20
4	20	20	30
5	20	20	50
6	20	20	75
7	20	10	35
8	20	40	35
9	10	20	35
10	40	20	35
11	10	10	35
12	30	30	35
13	40	40	35

Fluid: water

$D = 2 \text{ cm}$

Table 3.1 - Test Schedule

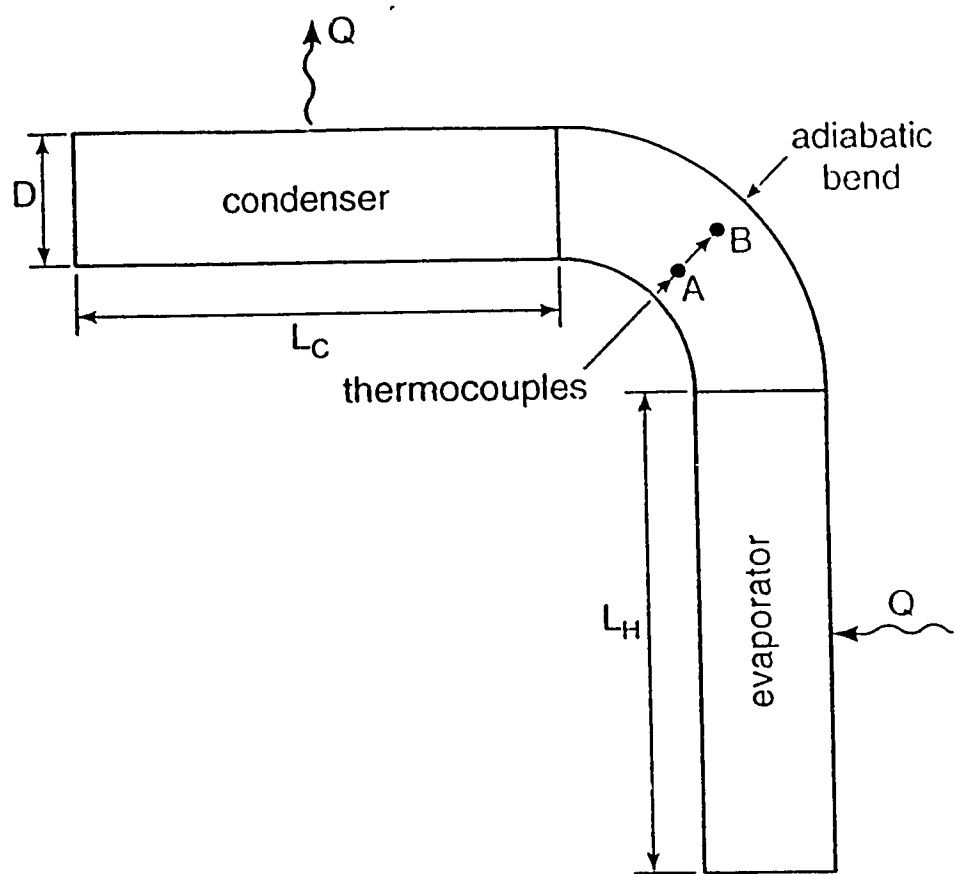


Fig. 3.1 Schematic of right-angled thermosyphon.

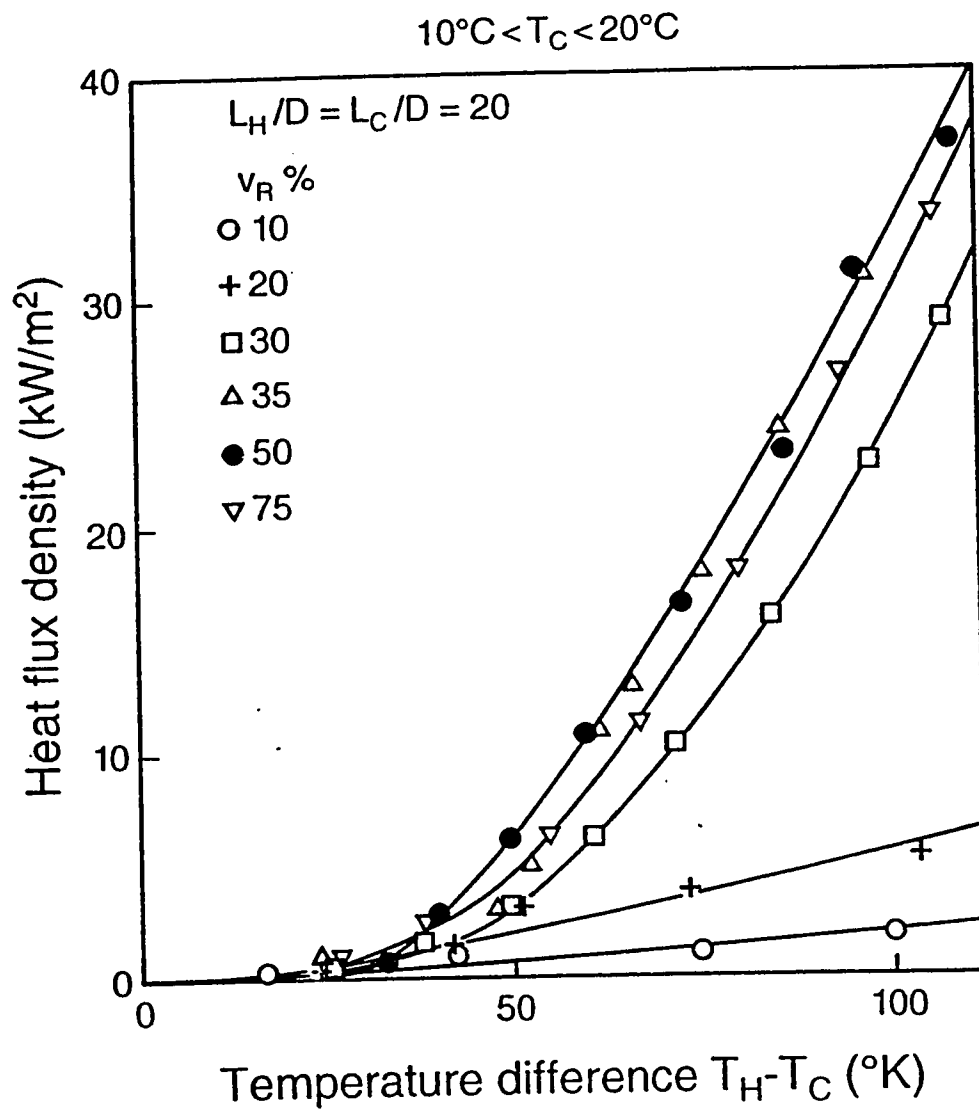


Fig. 3.2 Effect of filling quantity on heat transfer.

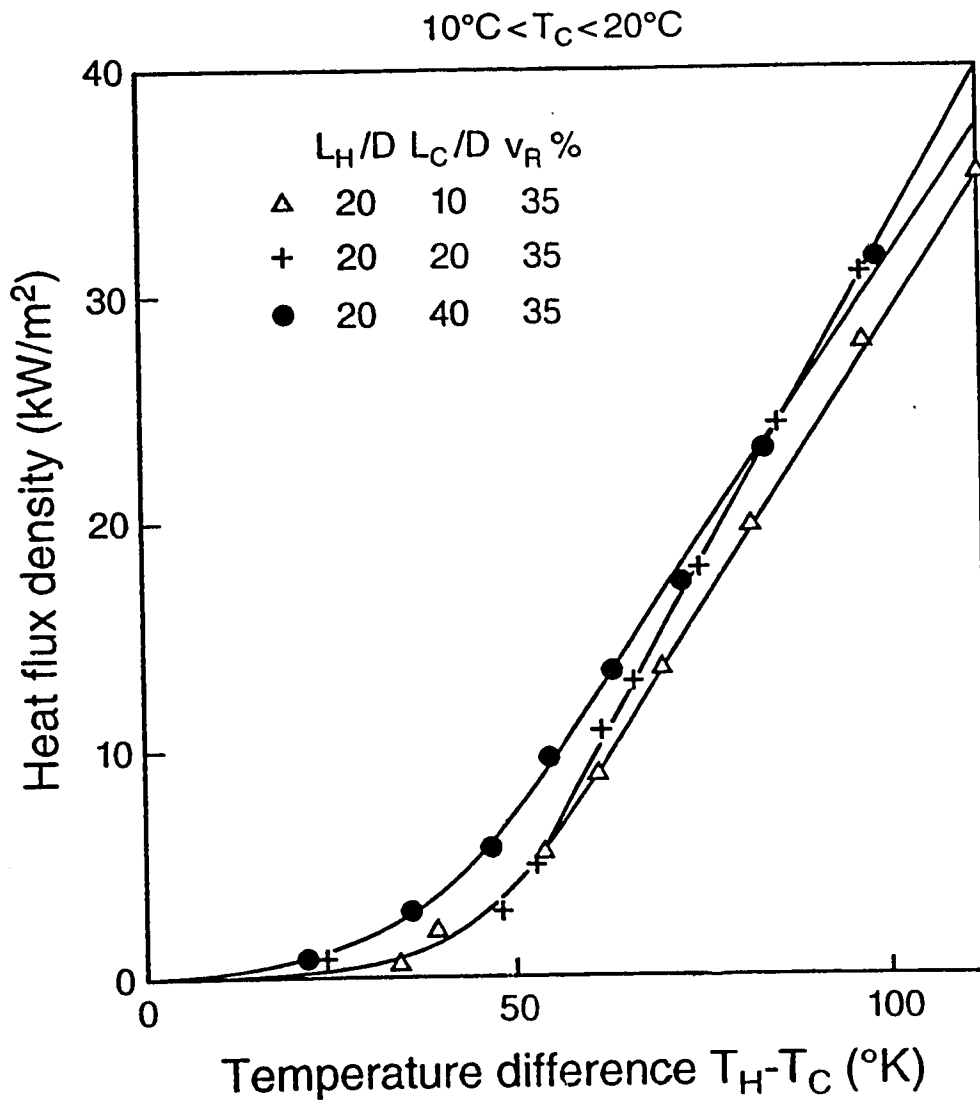


Fig.3.3 Effect of condenser length on heat transfer.

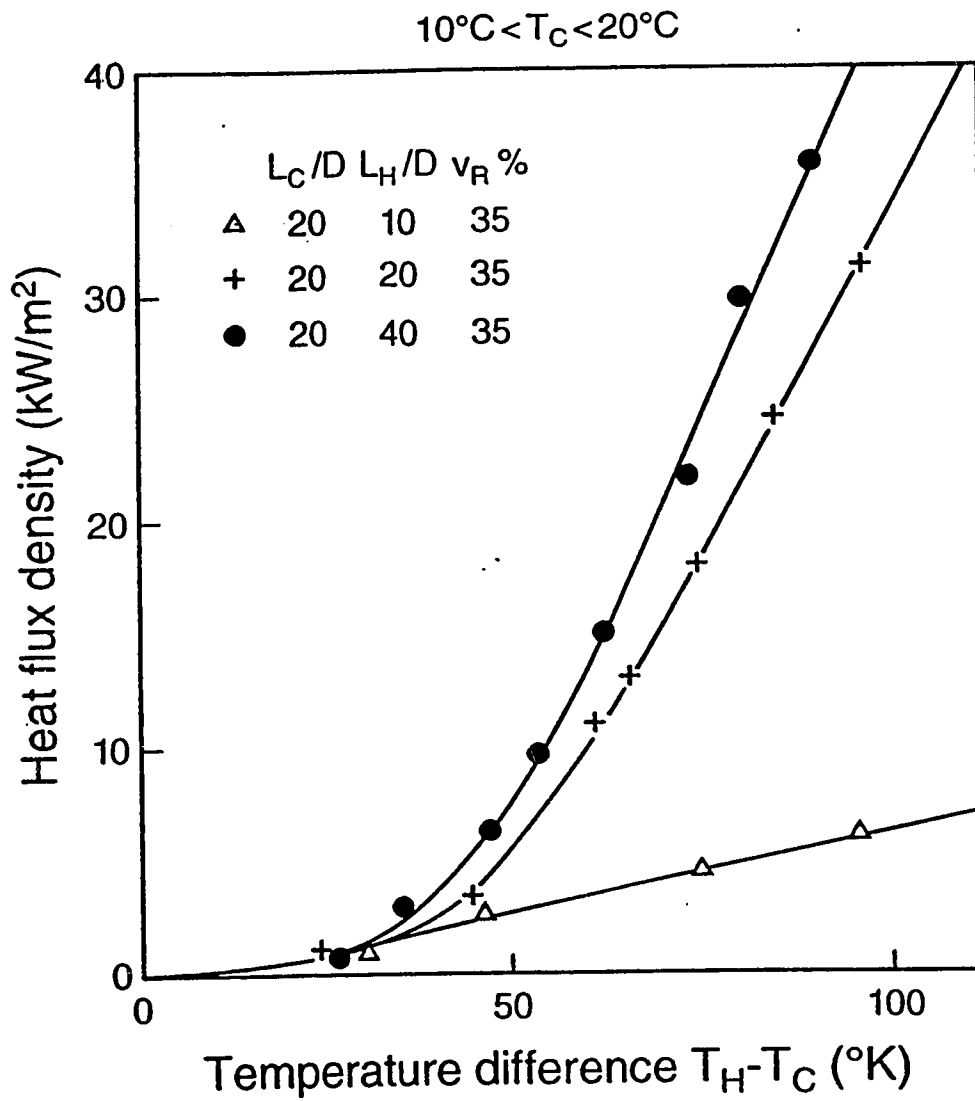


Fig. 3.4 Effect of evaporator length on heat transfer.

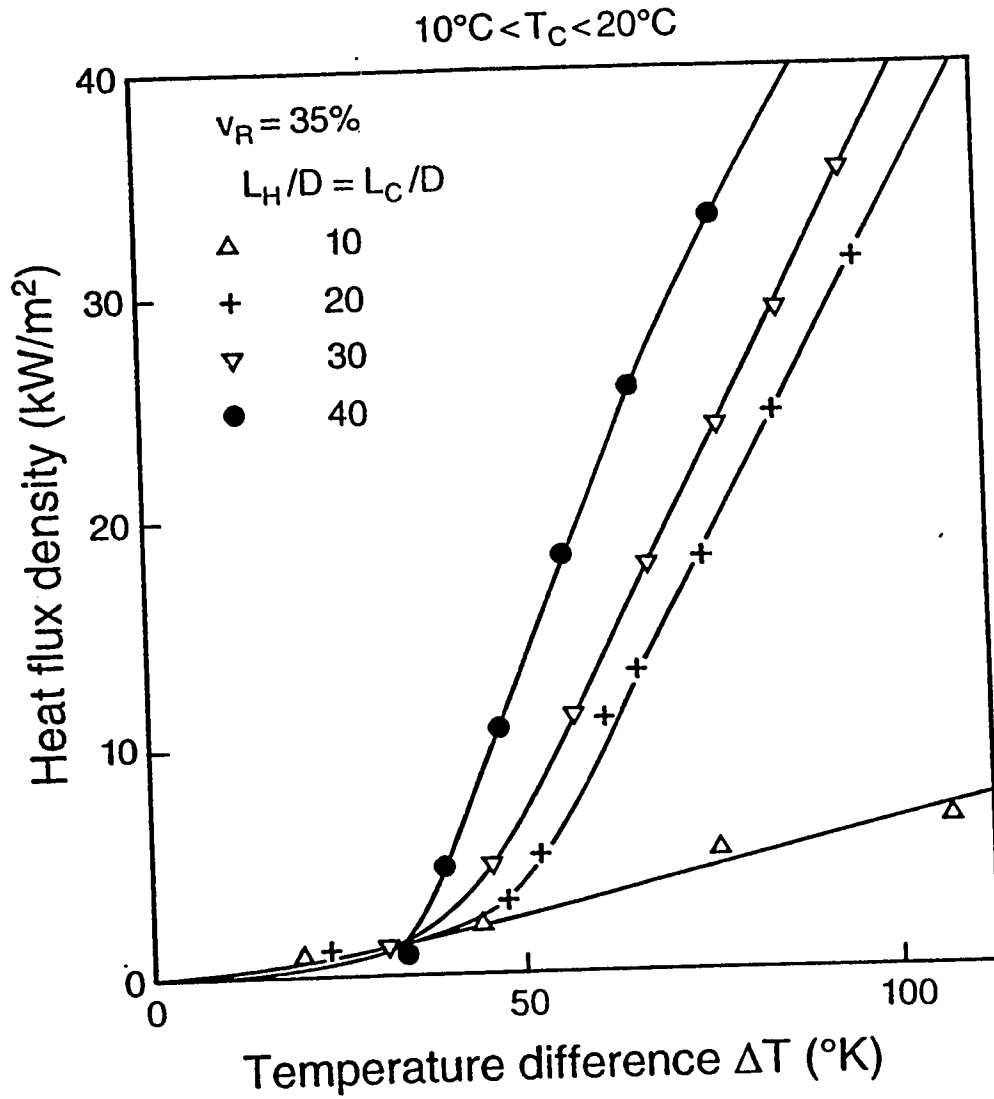


Fig. 3.5 Effect of length-diameter ratio on heat transfer.

References

- Long, E.L., 1963. The long thermopile. Proc. Int. Conf. on Permafrost, National Academy Sciences, Washington, pp. 487-491.
- Haynes, F.D. and Zarling, J.P., 1988. Heat transfer performance of commercial thermosyphons with inclined evaporator sections. Proc. 7th Int. Conf. on Offshore Mechanics and Arctic Engineering, Houston, Vol. IV. pp. 275-280.
- Lock, G.S.H., 1992. The Tubular Thermosyphon, Oxford University Press, New York.
- Wilson, C.H., Pope, D.H., Cundy, V.A., Nydahl, J.E., and Pell, K.M., 1978. A demonstration project for de-icing of bridge decks. Bridge Eng., Vol. 1, pp. 189-197.
- Vasiliev, L.L., 1989. Heat pipe research and development in the USSR. Heat Recovery Syst. CHP, Vol. 9(4) pp. 313-333.
- Tanaka, O., Yamakage, H., Ogushi, T., Murakami, M., and Tanaka, Y., 1982. Snow melting using heat pipes. Advances in Heat Pipe Technology. Pergamon Press, Oxford, Proc. 4th Int. Heat Pipe Conf., London 11-23.
- Lock, G.S.H., 1972. Some aspects of ice formation with special reference to the marine environment. Trans. North East Coast Inst. Eng. Shipbuild., Vol. 88, pp. 175-184.
- Lock, G.S.H., and Fu, J., 1992. Performance of a right-angled, evaporative thermosyphon. Proc. 11th Int. Conf. on Offshore Mechanics and Arctic

Engineering, Calgary, Vol. IV, pp. 145-148.

Lock, G.S.H. and Ladoon, D., 1991. Heat transfer in a right-angled thermosyphon. Proc. 10th Int. Conf. on Offshore Mechanics and Arctic Engineering, Stavanger, Vol. IV, pp. 261-266.

Negishi, K. and Sawada, T., 1983. Heat Transfer performance of an inclined two-phase closed thermosyphon. Int. J. Heat Mass Transfer, Vol. 26(2), pp. 1207-1213.

CHAPTER 4

THE INFLUENCE OF EVAPORATOR AND CONDENSER INCLINATION ON THE PERFORMANCE OF A RIGHT-ANGLED THERMOSYPHON

4.1. Introduction

The evaporative thermosyphon has a long history extending back well into the 19th century. However, it was only in the second half of this century that it was first considered as a device suitable for the control of soil temperatures. Long (1963) suggested that its ability to transfer large amounts of heat upward might be used to maintain soil in a frozen and subcooled state. Cold winter winds could thus provide a heat sink that would facilitate latent heat (cold) storage in the soil, thereby preserving its structural integrity, even during the succeeding summer thaw period.

Thus began the application of the thermosyphon to various foundation designs appropriate to northern regions where thermal erosion or permafrost degradation may pose a serious threat to the structural integrity of buildings, towers, roads, airstrips etc.

⁴A version of this chapter has been published in the Proceedings of the 12th International Conference on Offshore Mechanics and Arctic Engineering, Vol. IV: pp. 213-217, Glasgow, 1993.

(Haynes and Zarling, 1988). More recently, the device has found use in many other arctic and subarctic situations (Cheng and Zarling, 1990). Most notable among these are the storage of food (Fukuda et al., 1990) and the provision of an anti-icing or de-icing capability on various structures, vehicles and pieces of equipment which operate in a chilled atmosphere where wind and water combine to create massive amounts of surface ice (Lock, 1992).

The thermosyphon as a de-icing device acts as a thermal "superconductor" carrying heat from a natural or man-made source towards the surface on which ice has formed. This heat need only be sufficient to melt the ice immediately adjacent to the surface, thus enabling the bulk of the ice to be efficiently removed by simple mechanical means. Particular examples of this strategy are: the de-icing of bridge decks (Wilson et al., 1978); the de-icing of railway points (Vasiliev, 1989); the de-icing of paved surfaces (Tanaka et al., 1982); and the de-icing of shipboard surfaces (Lock, 1972).

In many of the above applications, the overall design may call for thermosyphon tubes which cannot be straight. In particular, it is common to find situations in which the tube must take a right angled form. In the de-icing of paved surfaces, for example, a horizontal condenser (located in the surface) lies above a vertical evaporator (collecting geothermal or electric heat). On the other hand, to maintain frozen soil beneath a building, a horizontal evaporator (lying in the soil) connects with a vertical condenser standing upright in the atmosphere. These are the two extreme orientations of the right angled thermosyphon.

This paper is an experimental study of the right-angled thermosyphon depicted in

Fig. 4.1. The work extends an earlier investigation (Lock and Fu, 1992) in which the basic performance of the device was explored. Here, we report a systematic investigation designed to provide the designer with a greater choice of configurations, including the limiting orientations mentioned above. At the same time, an attempt will be made to establish trends in thermodynamic and hydrodynamic behaviour resulting from changes in configuration. In this way, designers will be provided with insights that will help them when faced with other configurations in other circumstances.

4.2. Experiments

Since the apparatus has been fully described in the earlier paper (Lock and Fu, 1992), it will not be discussed in any detail here. It is sufficient to note that it consisted of a small bore (2 cm dia.) copper tube heated electrically in 20 cm lengths, and cooled with a water jacket, also in 20 cm lengths (see Fig.A1.1). The filling (water) was fixed at $v_R = 35\%$ of the evaporator volume. For a given difference between the evaporator wall temperature T_H and the condenser wall temperature T_C , the heat leakage, obtained from a calibration curve, was subtracted from the gross power supplied electrically to provide the net rate of heat transfer through the system.

Copper-constantan thermocouples were used throughout for the measurement of temperature. These were located at 5.5 cm intervals along the tube walls and in the room air (see Fig. A1.2).

Preparation, assembly and testing always followed the same routine. Firstly, the tubes were cleaned inside using benzene, alcohol and distilled water, in that order.

Secondly, a vacuum pump was connected to the apparatus and the air pressure lowered to about 1 kPa, i.e. near the triple point. With the apparatus sealed, several hours were then allowed to elapse to ensure that no leaks existed. Thirdly, a charge of water was introduced using a hypodermic syringe. Fourthly, the electric heater was switched on along with the vacuum pump. This purged the remaining air (and some water vapour) while the water boiled gently. The apparatus was then sealed prior to testing at subatmospheric pressure. Periodic checks were subsequently made to ensure that no air leakage had occurred.

The experiments consisted of plotting the heat flux density q (based on the heated surface area) versus the temperature difference $T_H - T_C$. Each wall temperature was calculated as the (spatial) average of at least twenty point readings. Once the full range of $T_H - T_C$ has been covered, the test was terminated and the procedure repeated (except the cleaning) after an adjustment had been made in the tube orientation.

There are, in general, three rotational degrees of freedom but in a uniform gravitational field any rotation about the vertical axis has no effect. Hence, the tube orientation may be described by two angles of inclination, as indicated in Fig. 4.1. Beginning with the evaporator vertical, the tilt angle ϕ_t was defined as the evaporator inclination in a vertical plane. The rotation angle ϕ_r was then measured about the evaporator tube axis O-A from a position in which the condenser is at its highest point, i.e. in the same plane as the evaporator. Bearing in mind symmetry and the need to keep the condenser above the evaporator, both angles need only be covered in the range $0 \leq \phi \leq \pi/2$.

The tests reported here were all conducted with water as the filling. While it is recognized that water could not be used in a subzero application, the behaviour investigated is representative of any fluid, including many refrigerants, which operates closer to its triple point than its critical point. To simulate this behaviour a simple set of auxiliary experiments was undertaken using air bubbling into water inside a right angled, transparent tube having the same dimensions. Since

$$\dot{q} A_H = \dot{m} \lambda \quad (4.1)$$

where A_H is the evaporator tube surface on which the heat flux density \dot{q} is based, the corresponding mass flow rate \dot{m} in the simulated isothermal experiment could be calculated and set by adjusting and matching the upward air bubbling rate to the downward water flow rate.

4.3. Discussion of Results

Figure 4.2 shows various test runs in which the heat flux density \dot{q} is plotted against $T_H - T_C$. These particular runs were undertaken with zero rotation, i.e. the condenser and evaporator lay in the same plane. As indicated, the tilt was varied over the full range of 90° . This figure is typical of many others obtained while tilt and rotation were systematically varied. In general, changes in orientation shifted the \dot{q} versus ΔT curves up or down, but not monotonically with respect to ϕ_t except over a small range of angles. As the figure shows, the effects of orientation were obscured. It was therefore decided to construct cross plots from smooth curves drawn through the raw $\dot{q} - \Delta T$ data.

The cross plots thus obtained provide a composite picture of heat transfer behaviour. Three plots in particular provide valuable insights. The first of these is shown in Fig. 4.3. As indicated, these data were obtained with $\phi_c = 90^\circ$, i.e. a horizontal condenser. They therefore reflect the effect of inclination on the evaporator while the condenser behaviour is nominally fixed.

From observations on the simulated experiments, three régimes may be identified in Fig. 4.3. For shallow tilt angles e.g. $\phi_i \lesssim 30^\circ$, the effect of tilt is very small. In these conditions, the lateral component of the gravity acceleration plays only a small role. Bubbly flow in the lower reaches of the tube gradually becomes plug flow as the result of bubble coalescence increasing with height (see Fig. A6.5). Near the top of the evaporator, plug flow is replaced by churn flow. In the condenser, a weak rivulet drains towards the evaporator (see Fig. A6.6).

For intermediate tilt angles, e.g. $30^\circ \lesssim \phi_i \lesssim 75^\circ$, the effect of the lateral component of the gravitational acceleration is to improve the heat transfer rate by establishing a different flow pattern. This consists of a bifilamental circulation in which vapour bubbles are essentially confined to the upper evaporator surface while replenishing liquid dominates near the lower surface. Even so, bubbly flow near the bottom of the evaporator is still converted to plug flow higher up the tube.

Beyond $\phi_i \approx 75^\circ$, the flow pattern changes yet again. The lateral component of the gravitational acceleration now dominates the flow. For this filling ($v_R = 35\%$), coalescence near the upper storage of the evaporator tube creates a wavy slug flow

moving in opposition to the returning liquid beneath (see Fig. A6.7). In the presence of a greatly reduced longitudinal component of the gravitational acceleration, the circulation rate, along with the heat transfer rate, is also reduced. As $\phi_t \rightarrow 90^\circ$, the weak circulation in the evaporator is exacerbated by an increasing tendency to flood the condenser (see Fig. A6.8), thereby reducing the overall heat transfer rate rapidly, as indicated in Fig. 4.3.

A corresponding survey of condenser behaviour is provided by the data in Fig. 4.4 for which the evaporator is held fixed in the horizontal position. Here again, three régimes are evident, the inclination ranges being remarkably similar to those noted above. As rotation increases, very little change occurs until, near $\phi_r = 30^\circ$, the lateral component of the gravitational acceleration comes into play, principally by thinning the condensate film which tends increasingly to move round the tube surface rather than along it. The enhancing effect of a shorter condensate path continues until $\phi_r \approx 60^\circ$ at which point the wavy-plug flow in the evaporator begins to enter the mouth of the condenser. The associated deterioration in circulation rate increases as ϕ_r is increased further; at the same time, the rivulet draining the condenser becomes weaker. As Fig. 4.4 reveals, the overall result is a rapid reduction in heat transfer rate as $\phi_r \rightarrow 90^\circ$.

Much of the above discussion helps explain the data shown in Fig. 4.5. These were obtained by inclining the thermosyphon with the evaporator and condenser held in the same plane. For small tilts, the evaporator performance changes little but more efficient drainage in the condenser creates a rise in overall performance up to $\phi_t = 30^\circ$. In the range $30^\circ \leq \phi_t \leq 70^\circ$, increases in evaporator performance are evidently offset

by decreases in condenser performance, the net result being a fairly constant heat transfer rate. Only in the range $70^\circ \leq \phi_t \leq 90^\circ$ does behaviour change abruptly and unexpectedly. As $\phi_t \rightarrow 90^\circ$, the performance of the evaporator alone would be expected to decrease rapidly, but Fig. 4.5 reveals a short-lived rise preceding a local maximum before the anticipated deterioration actually occurs. At the time of writing, we are unable to explain this apparent anomaly.

Figures 4.3, 4.4, and 4.5 are limiting curves for the three-dimensional surfaces

$$\dot{q} = \dot{q}(\phi_r, \phi_t, \Delta T) \quad (4.2)$$

A fourth limit is given when $\phi_t = 0$ for all ϕ_r but this corresponds to rotation of the condenser when the evaporator is vertical; no change in heat transfer then occurs. It was found that equation (4.2) formed a family of surfaces separated by the level of ΔT . Fig. 4.6 shows a representative set of contours with $\Delta T = 70$ K. The top edge corresponds to Fig. 4.3, the bottom edge to Fig. 4.5 and the right hand edge to Fig. 4.4. These contours reveal the complex effect of orientation on heat transfer and, in particular, highlight the regions important to designers. Apart from locating the regions of high performance they also reveal zones where the gradient is either low or high. A low gradient indicates a fairly constant performance under changing orientation, as when a ship pitches and rolls. A high gradient, on the other hand, provides the designer with the ability to create a thermal switch by a simple shift in orientation; for example, by varying ϕ_t in the range $80^\circ < \phi_t < 100^\circ$ when $\phi_r \lesssim 45^\circ$.

4.4. Conclusions

The paper has attempted to provide a systematic survey of the effect of orientation on the heat transfer performance of a right angled, evaporative thermosyphon. Using a small bore tube containing water, experimental data have been obtained for a complete range of inclinations of the evaporator and condenser. The study has been defined in terms of the tilt angle (of the evaporator) and the rotational angle (of the condenser).

With the condenser horizontal, the effect of tilting the evaporator may be divided into three régimes. These may be described in terms of gradual alterations in the evaporator circulation pattern, as observed in an accompanying simulation study. Likewise, visual observations may be used to explain the effect of rotating the condenser with the evaporator horizontal. As a general rule, the more vigorous the circulation the higher the heat transfer rate. Flow impedances and the reduction of Archimedean buoyancy forces thus explain the observed reductions in heat transfer rate.

A representative contour map of heat flux density on the tilt-rotation plane has been constructed from a series of plots of \dot{q} versus ΔT for each of a series of tilt and rotation angles. This revealed the overall complexity of the hydrodynamics and thermal behaviour of the right angled thermosyphon but also provided useful guidance to the designer. In particular, the regions of high performance were delineated; these are especially important where the effect of inclination is low. In addition, regions where performance varies rapidly with inclination provide the designer with a thermal switch capability.

Acknowledgements

This work was conducted under the auspices of the Natural Sciences and Engineering Research Council of Canada to whom we are indebted. We would also like to thank the technicians and machinists of the Department of Mechanical Engineering for their help.

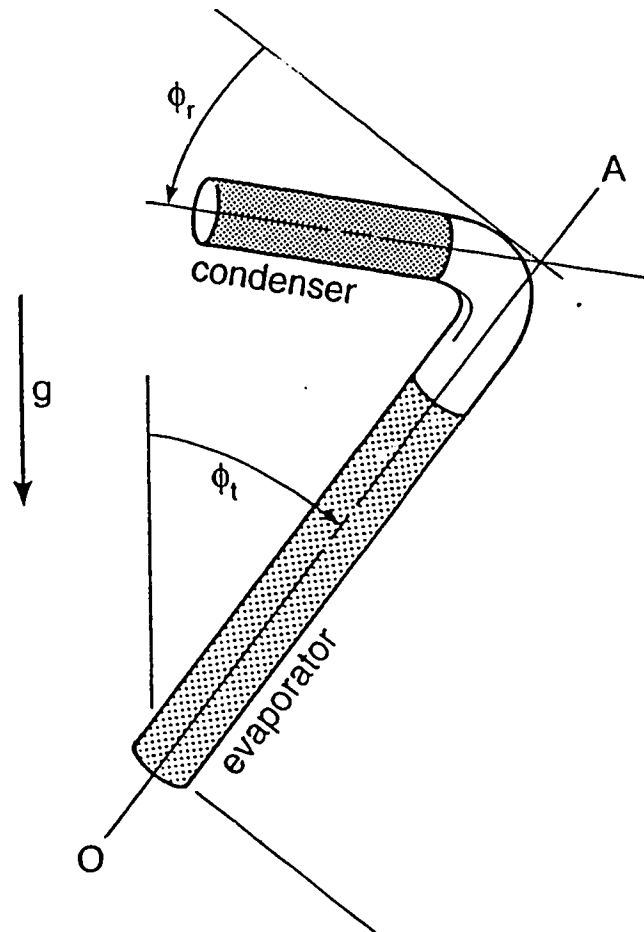


Fig. 4.1. Schematic representation inclined of right-angled thermosyphon.

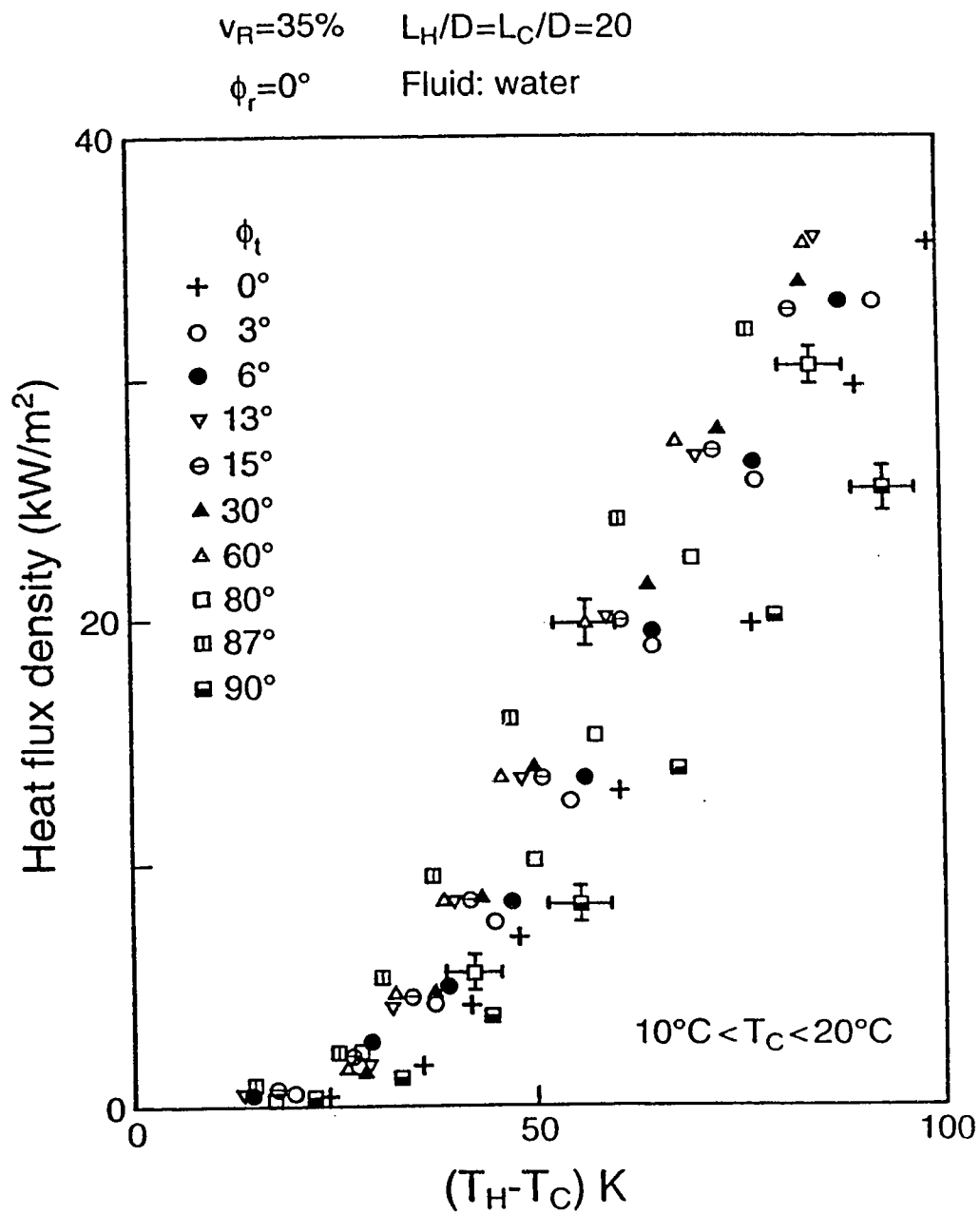


Fig. 4.2 The effect of tilt on heat transfer without rotation.

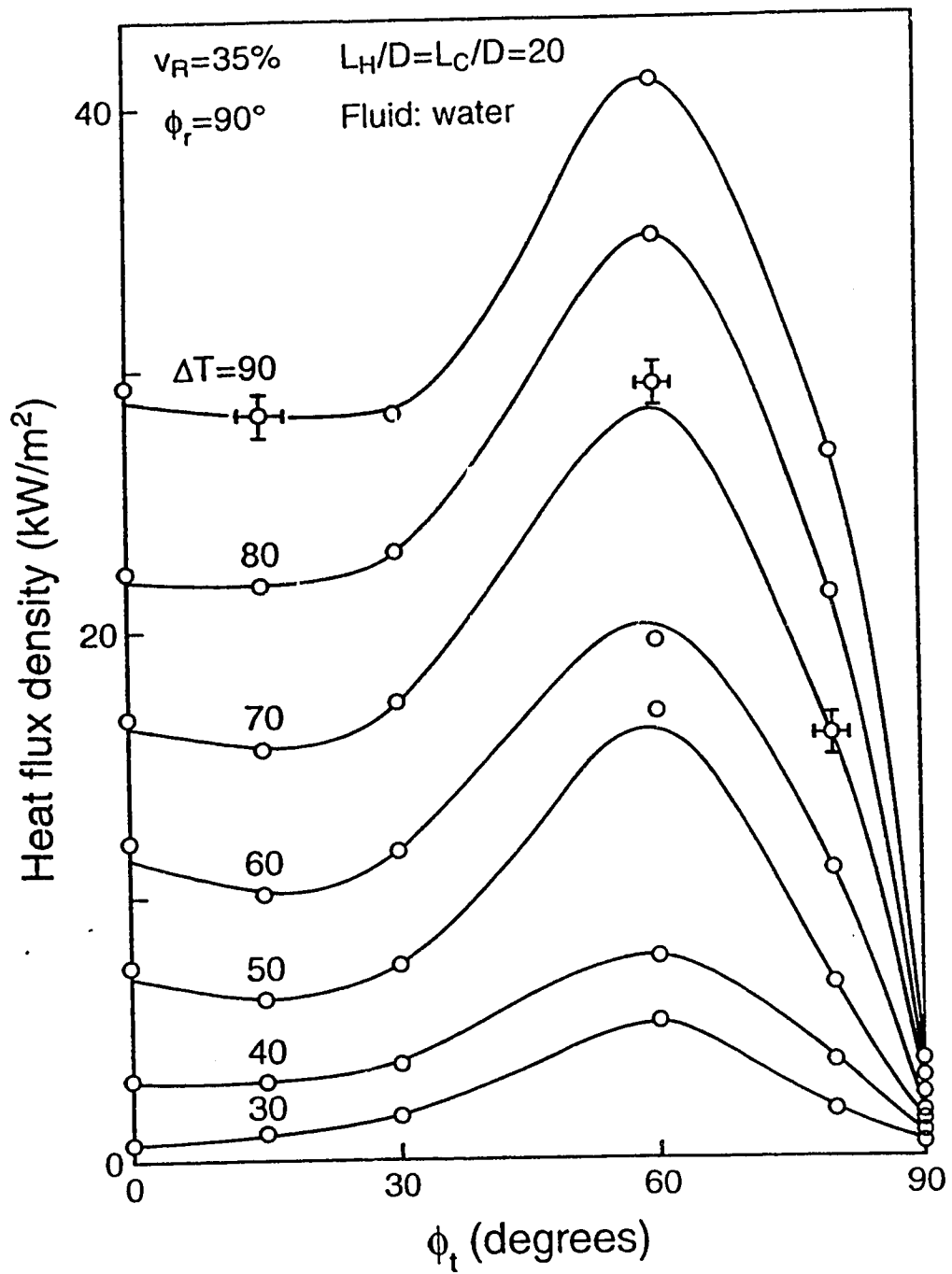


Fig. 4.3 Effect of tilt on heat transfer with a horizontal condenser.

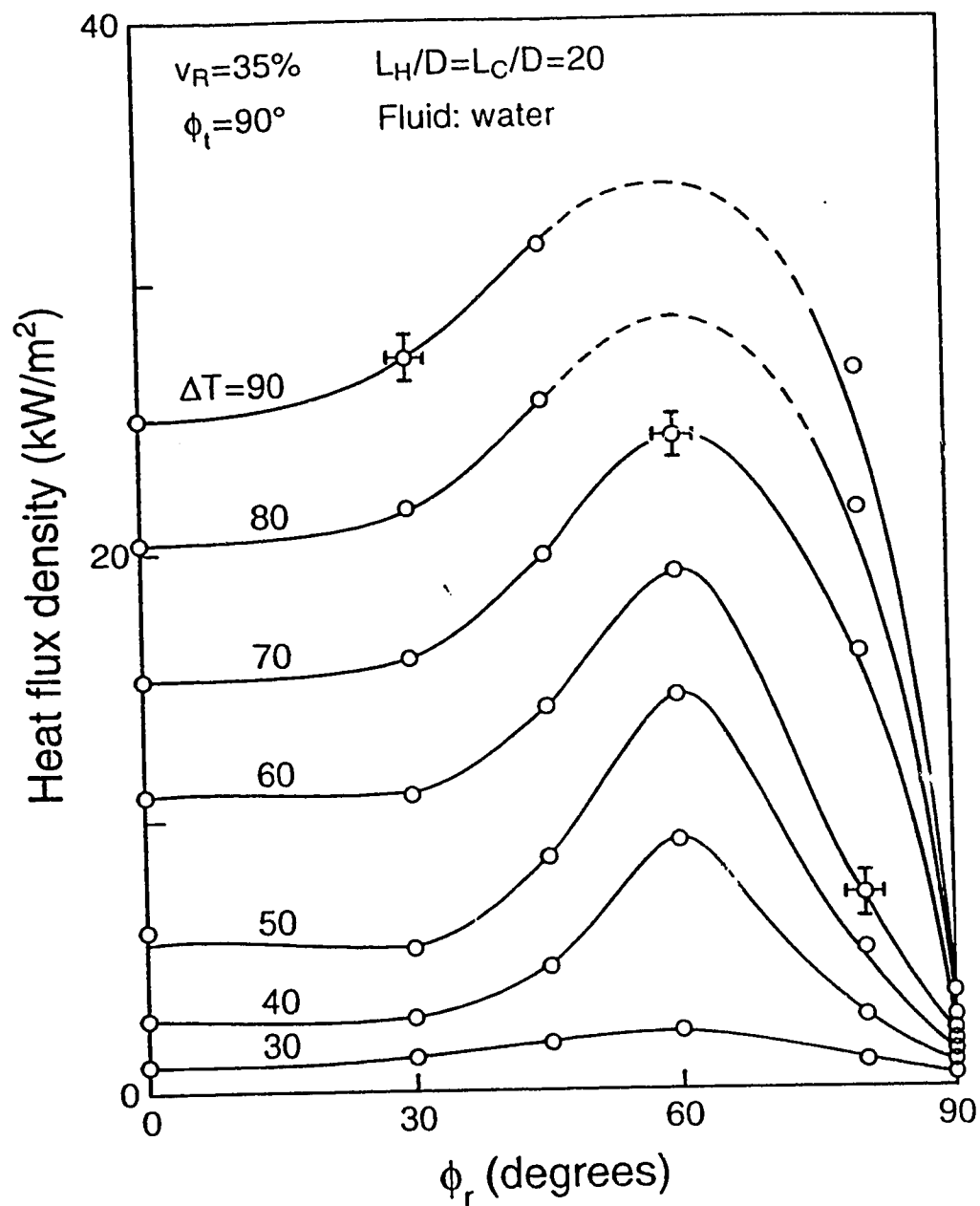


Fig. 4.4 Effect of rotation on heat transfer with a horizontal evaporator.

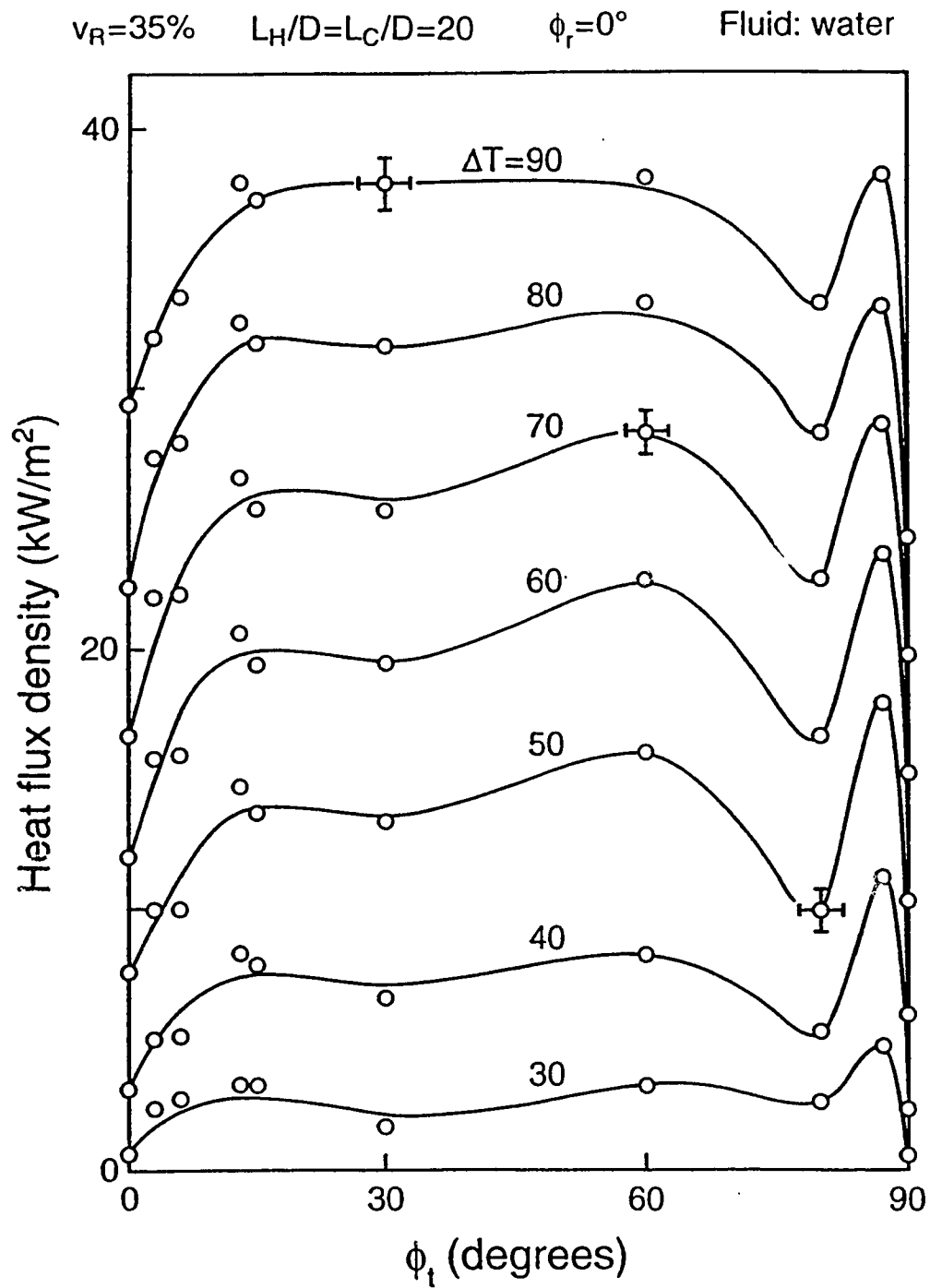


Fig. 4.5 Effect of tilt on heat transfer with $\phi_r = 0^\circ$.

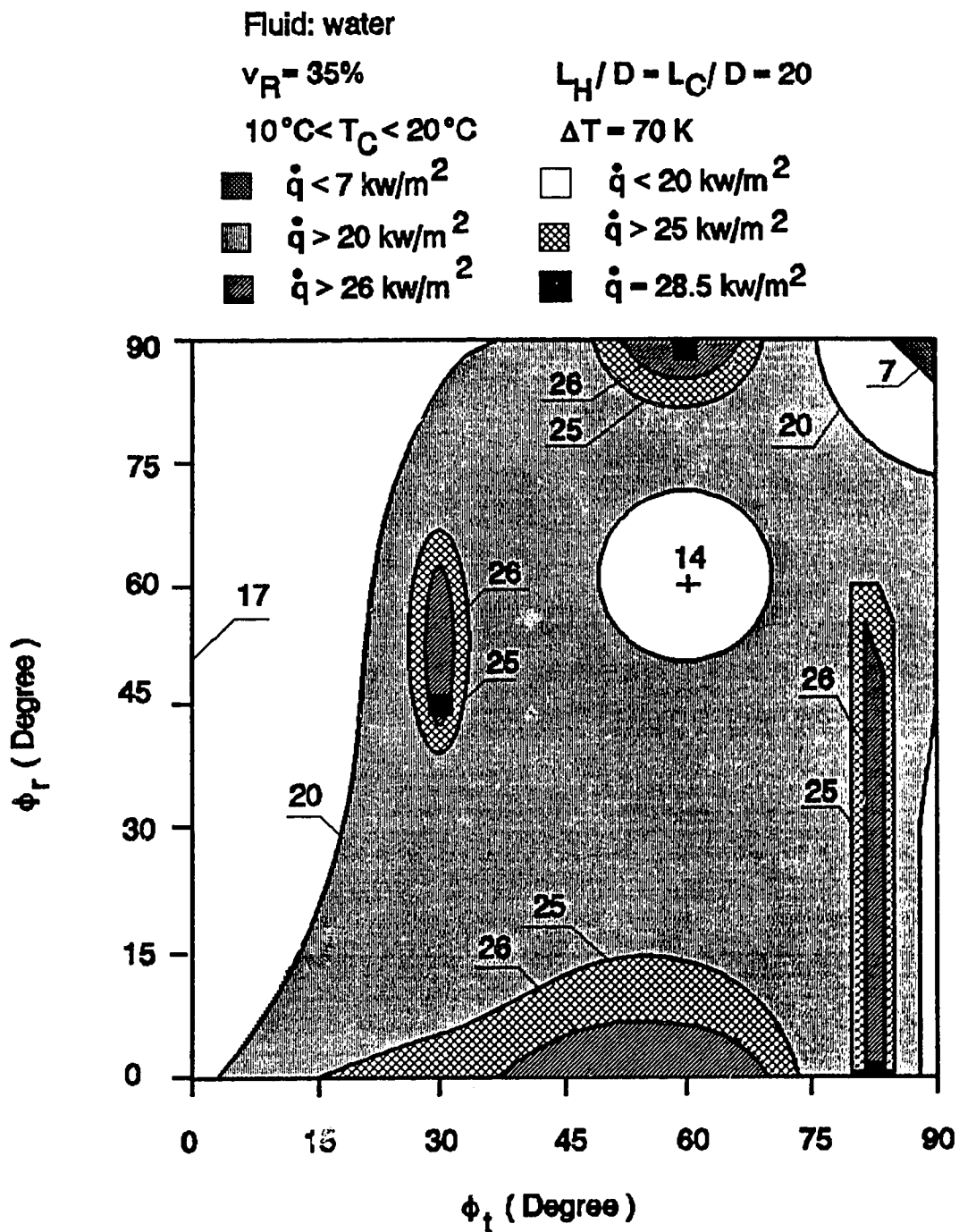


Fig. 4.6 Typical heat transfer contours showing the effect of tilt and rotation.

References

- Long, E.L., 1963, The long thermopile, Proc. Permafrost Int. Conf., pp. 487-491.
- Haynes, F.D. and Zarling, J.P., 1988, Thermosyphons and foundation design in cold regions, Cold Regions Sci. Technol., Vol. 15: pp. 251-259.
- Cheng, K.C. and Zarling, J.P., 1990, Applications of heat pipes and thermosyphons in cold regions, Proc. 7th Int. Heat Pipe Conf., Minsk.
- Fukuda, M. et al., 1990, Development of an artificial permafrost storage using heat pipes, Proc. 7th Int. Heat Pipe Conf., Minsk.
- Lock, G.S.J., 1992, The Tubular Thermosyphon, Oxford University Press.
- Wilson, C.H. et al., 1978, A demonstration project for de-icing of bridge decks. Bridge Engineering Vol. 1: pp. 189-197.
- Vasiliev, L.L., 1989, Heat pipe research and development in the USSR, Heat Recovery Systems and CHP, Vol. 9 (4): pp. 313-333.
- Tanaka, O., Yamakage, H., Ogushi, T., Murakami, M., and Tanaka, Y., 1981, Snow melting using heat pipes, Advances in Heat Pipe Technology, pp. 11-24, Pergamon Press.
- Lock, G.S.H., 1972, Some aspects of ice formation with special reference to the marine environment, Trans. North East Coast Inst. Eng. Shipbuild, Vol. 88, pp. 175-184.
- Lock, G.S.H. and Fu, J., 1992, Performance of a right-angled, evaporative thermosyphon, Proc. 11th Int. Conf. on Offshore Mech. and Arctic Eng., ASME Vol. IV: pp. 145-148.

CHAPTER 5

SUMMARY AND RECOMMENDATIONS

5.1. Summary

Heat transfer characteristics of the evaporative elbow thermosyphon have been investigated experimentally in three areas to further our understanding of its behaviour. In the first area an experimental study of the thermosyphon was performed with an emphasis on filling quantities. As concluded in Chapter 3, thermosyphon behaviour fell mainly in three filling regimes. To avoid the pool dryout, the filling must be large enough to create a flooding limit with the evaporator filled with a two-phase boiling mixture.

The second work of this thesis covered the tests of the influence of tube length-diameter parameters on the heat transfer performance. It was observed from the tests that the evaporator length-diameter ratio, L_H/D , had a significant influence on the heat transfer rate while the effect of condenser length-diameter ratio, L_C/D , was relatively small.

The third contribution was in developing a systematic view of the influence of the tube orientation on the heat transfer rate. With changing the angles of tilt and rotation, which were defined in Chapter 4, the experimental results revealed the complex hydrodynamic behaviour. A typical heat transfer contour represented this complexity and

provided useful information for application.

5.2. Recommendations for Further Study

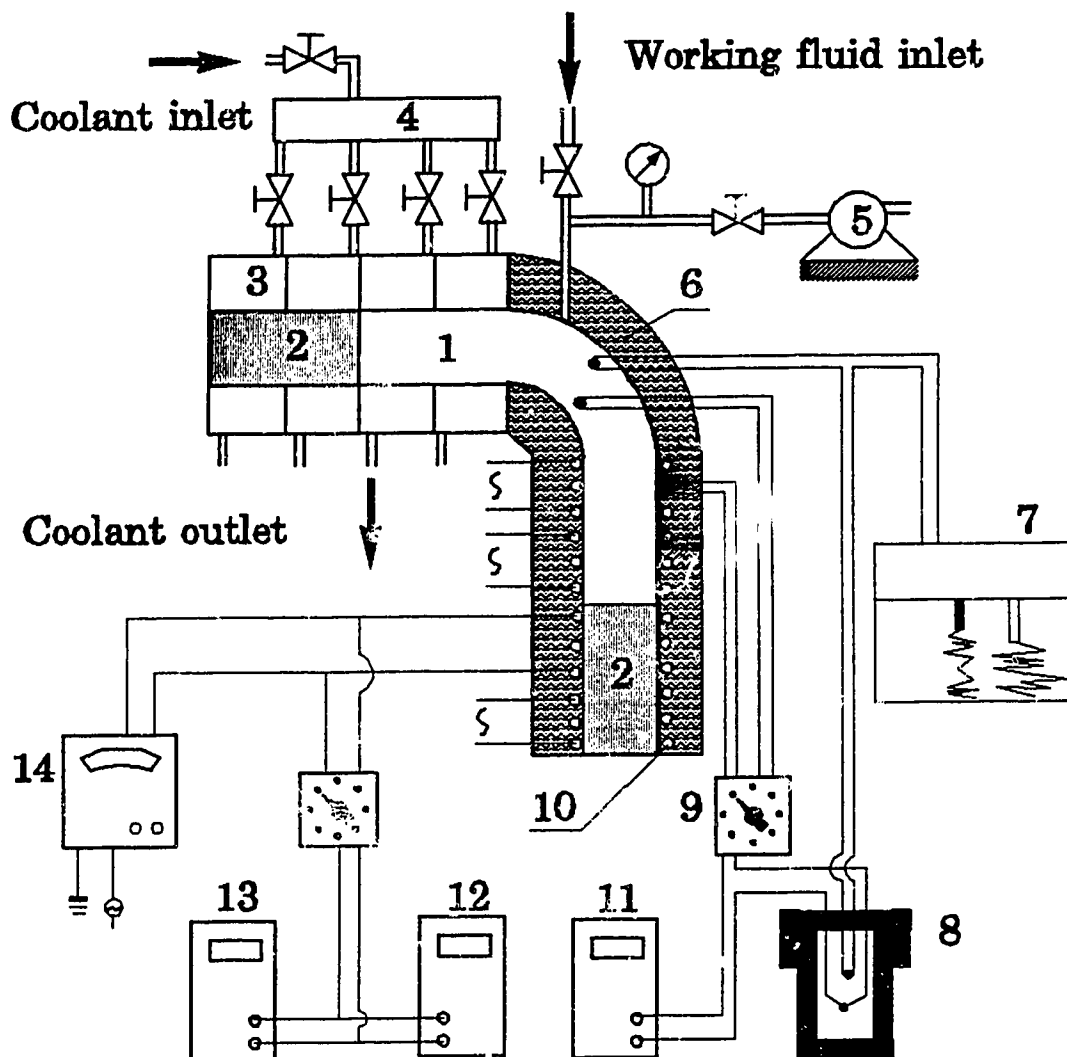
The present investigation of the elbow thermosyphon has raised several questions on this type of device. In order to establish a better understanding of the thermosyphon, the following areas are recommended for further study:

- 1) To interpret the heat transfer characteristics in the thermosyphon, visual observation with a transparent tube is required to show the heat transfer mechanisms and flow or phase change phenomena which control its performance.
- 2) A detailed investigation into the pressure influence on its evaporative behaviour, especially near the critical state.
- 3) Although water is a suitable working media for evaporation and condensation processes, it is understood that fluid properties can affect the heat transfer performance. A comparative investigation of different fluids is recommended.
- 4) A detailed study on the effect of incondensable gases is required to determine quantitatively the influence on overall device performance and to establish the influence on the heat transfer limit of the thermosyphon.

APPENDIX 1

ARRANGEMENT OF

THE EXPERIMENTAL APPARATUS



- | | | | |
|-------------------|-----------------------|--------------------|----------------|
| 1. Testing tube; | 2. Acrylic piston; | 3. Cooling jacket; | 4. Divider; |
| 5. Vacuum pump; | 6. Insulation; | 7. Chart recorder; | 8. Thermos; |
| 9. Switching box; | 10. Heater tape; | 11. Multimeter; | 12. Voltmeter; |
| 13. Ammeter; | 14. Power controller. | | |

Fig. A1.1. Arrangement of the experimental apparatus.

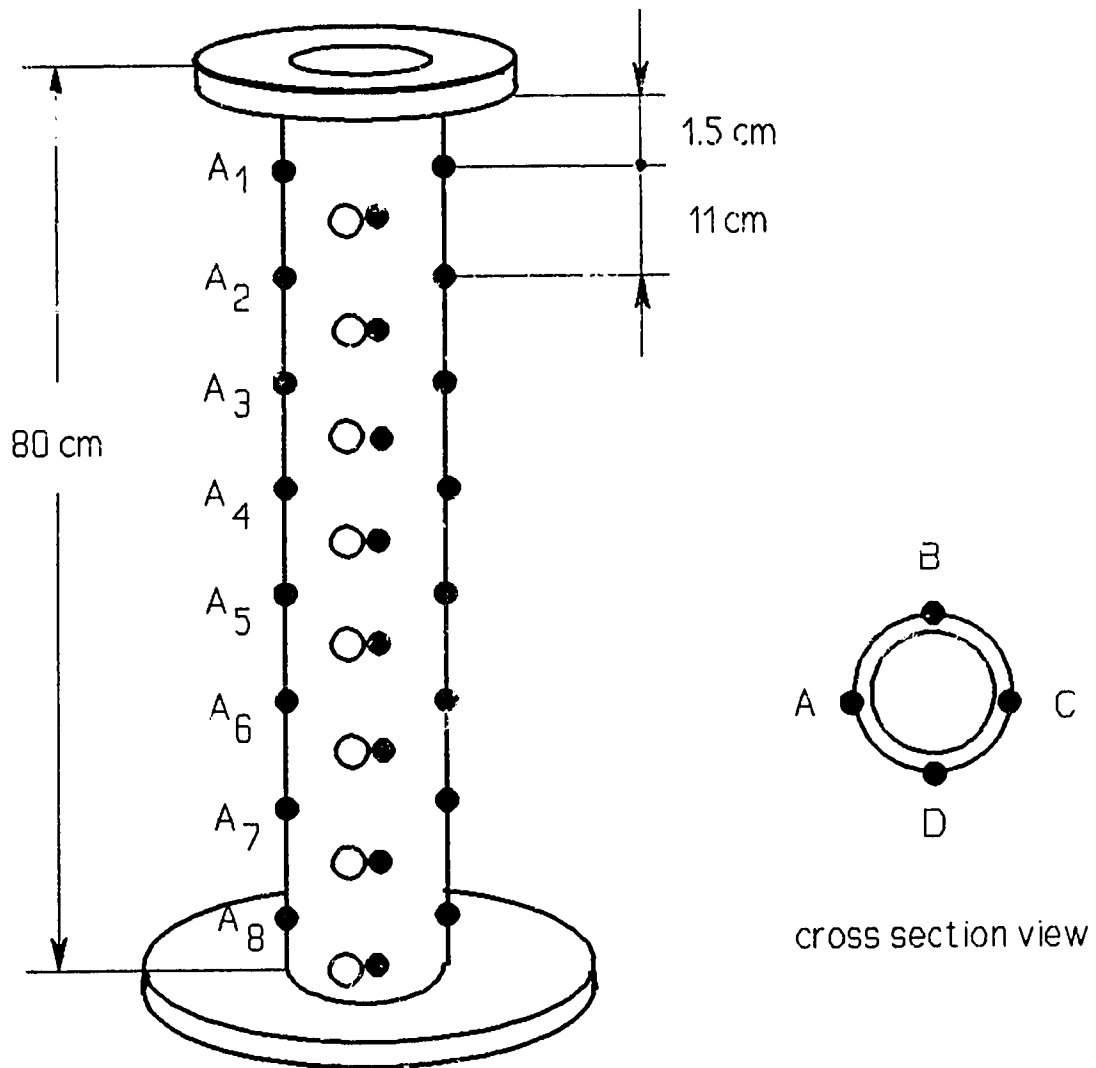


Fig. A1.2. Thermocouple arrangement and location.

APPENDIX 2

CALIBRATION CURVES

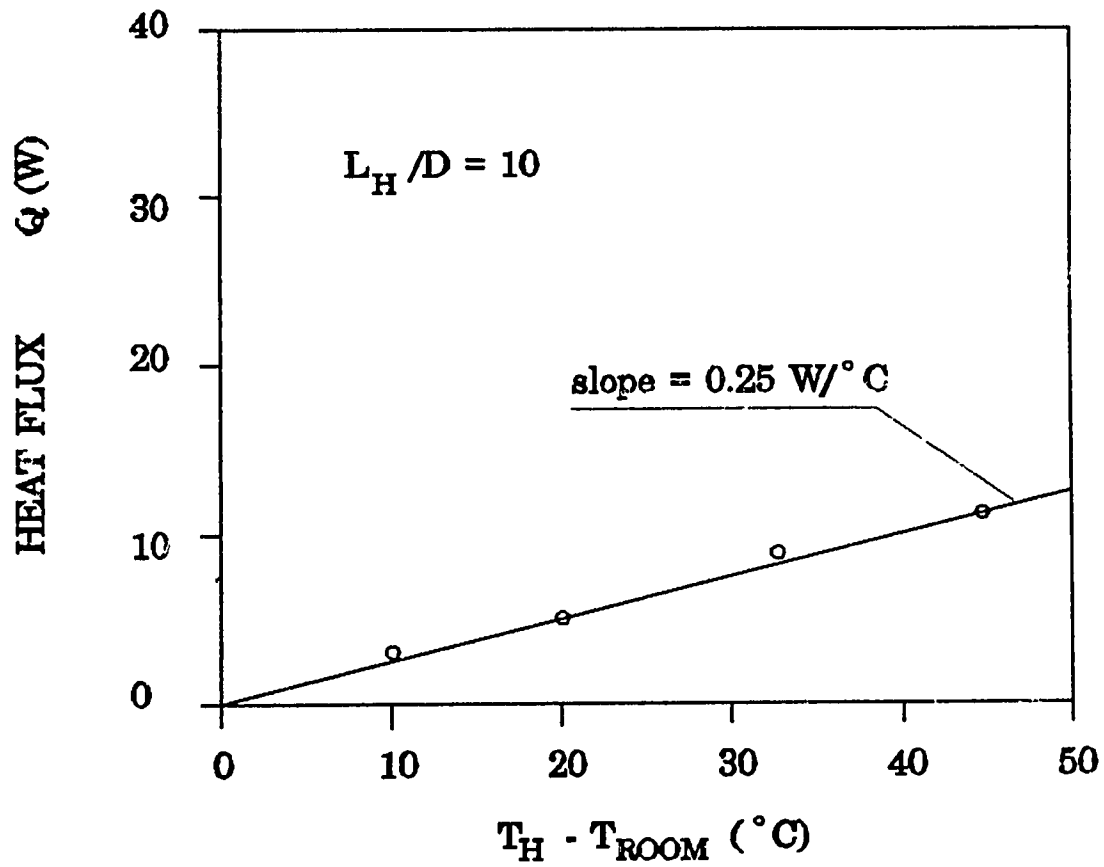


Fig. A2.1. Calibration curve for $L_H/D = 10$.

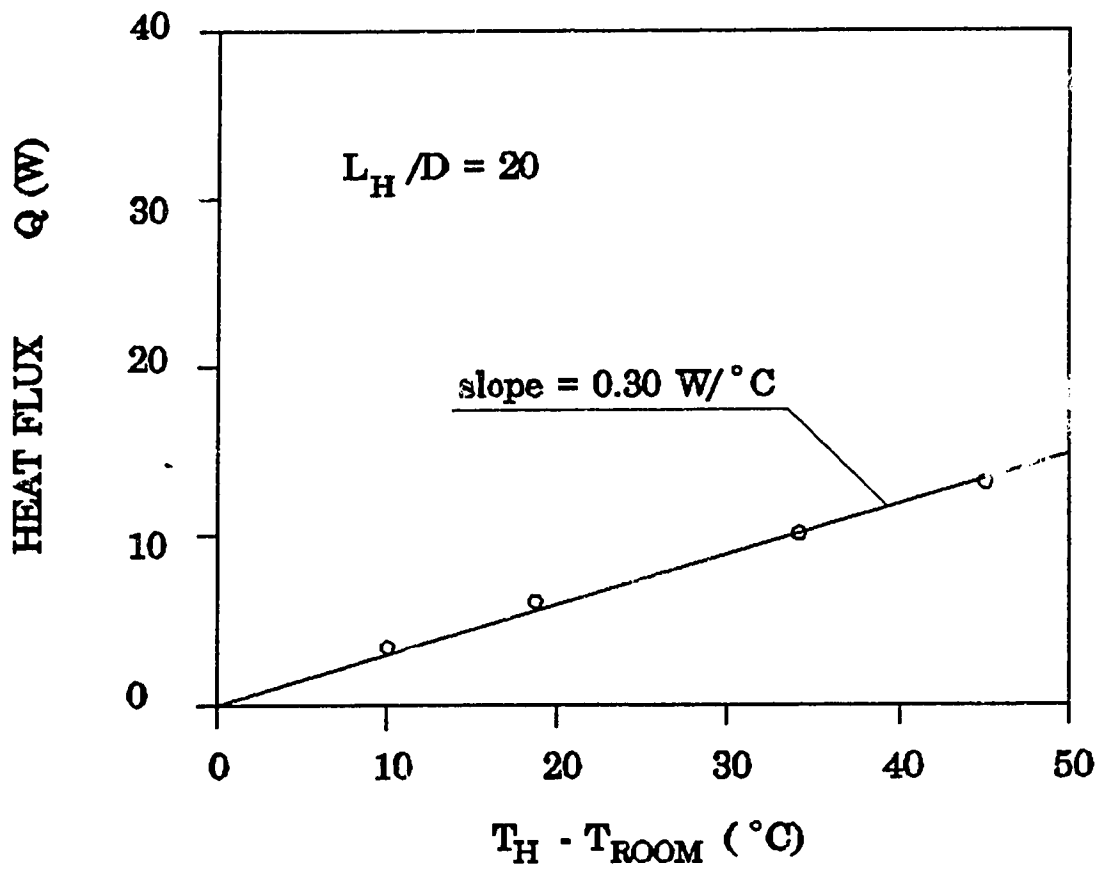


Fig. A2.2. Calibration curve for $L_H/D = 20$.

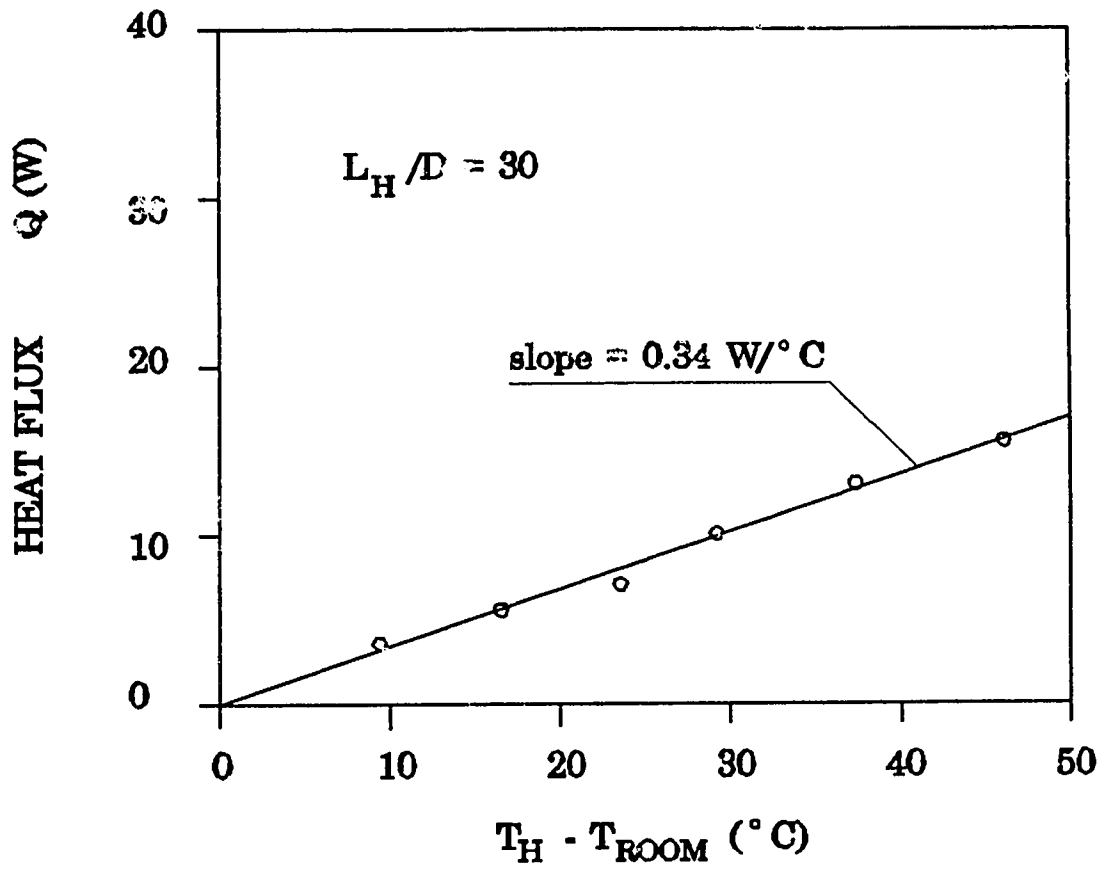


Fig. A2.3. Calibration curve for $L_H/D = 30$.

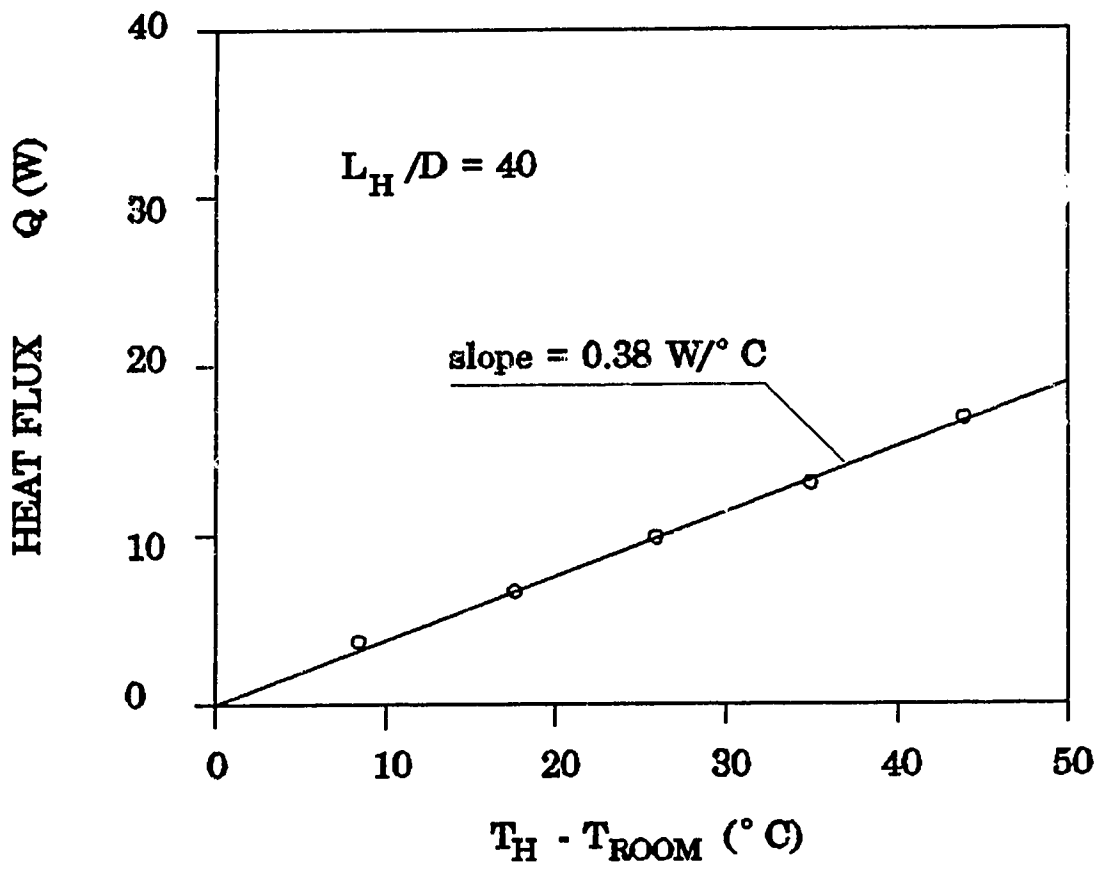


Fig. A2.4. Calibration curve for $L_H/D = 40$.

APPENDIX 3

EXPERIMENTAL DATA

1. Experiments of Filling Charge

Table A3.1. $v_R = 10\%$

Test No.	T_H (°C)	T_C (°C)	$T_H - T_C$ (°C)	T_{ROOM} (°C)	Q_G (W)	Q_N (W)	\dot{q} (W/m ²)
1	42.2	12.8	29.4	23.5	14.2	8.54	341.6
2	68.0	12.8	55.2	23.5	40.2	26.80	1072.0
3	114.0	13.5	100.5	23.5	80.1	52.95	2118.0

Table A3.2. $v_R = 20\%$

Test No.	T_H (°C)	T_C (°C)	$T_H - T_C$ (°C)	T_{ROOM} (°C)	Q_G (W)	Q_N (W)	\dot{q} (W/m ²)
1	35.1	11.2	23.9	23.0	12.6	9.00	360.0
2	53.6	11.2	42.4	23.0	39.2	30.00	1200.0
3	62.6	11.2	51.4	23.0	90.7	78.80	3152.0
4	116.0	11.4	104.6	23.0	173.6	145.70	5828.0

Table A3.3. $v_R = 35\%$

Test No.	T_H (°C)	T_C (°C)	$T_H - T_C$ (°C)	T_{ROOM} (°C)	Q_G (W)	Q_N (W)	\dot{q} (W/m ²)
1	39.4	12.0	27.4	23.5	26.1	21.3	852.0
2	50.0	12.0	48.0	23.5	73.5	65.6	2625.0
3	65.6	12.0	53.6	23.5	138.8	129.2	5168.0
4	74.4	12.0	62.4	23.5	216.3	201.0	8040.0
5	82.5	12.0	70.5	23.5	321.0	303.3	12132.0
6	92.5	12.5	80.0	23.5	442.1	421.4	16856.0
7	107.7	13.0	94.7	23.5	633.8	608.5	24340.0

Table A3.4. $v_R = 50\%$

Test No.	T_H (°C)	T_C (°C)	$T_H - T_C$ (°C)	T_{ROOM} (°C)	Q_G (W)	Q_N (W)	\dot{q} (W/m ²)
1	43.8	11.0	32.8	23.0	27.4	21.20	848.0
2	52.1	12.0	40.1	23.0	83.1	74.40	2976.0
3	60.9	11.2	49.7	23.0	169.6	158.21	6328.0
4	71.0	11.3	59.7	23.0	287.2	272.80	10912.0
5	84.2	11.5	72.7	23.0	438.3	419.90	16796.0
6	98.0	11.7	86.3	23.0	608.3	585.80	23432.0
7	107.5	12.9	94.6	23.0	808.6	783.25	31332.0
8	131.8	14.7	117.1	23.0	1003.0	970.35	38812.0

Table A3.5. $v_R = 75\%$

Test No.	T_H (°C)	T_C (°C)	$T_H - T_C$ (°C)	T_{ROOM} (°C)	Q_G (W)	Q_N (W)	\dot{q} (W/m ²)
1	58.0	20.0	38.0	25.0	70.3	60.4	2416.0
2	75.0	20.0	55.0	25.0	173.8	158.8	6352.0
3	88.1	21.0	67.1	25.0	302.2	283.3	11332.0
4	102.0	22.0	80.0	25.0	474.7	451.62	18064.0
5	116.0	22.5	93.5	25.0	696.3	669.0	26760.0

2. Experiments of Tube Geometry

Table A3.6. $L_C/D = 20, L_H/D = 10.$

Test No.	T_H (°C)	T_C (°C)	$T_H - T_C$ (°C)	T_{ROOM} (°C)	Q_G (W)	Q_N (W)	\dot{q} (W/m ²)
1	43.3	12.5	30.8	24.0	15.7	10.9	867.7
2	58.5	12.5	43.0	24.0	42.2	33.6	2675.4
3	129.0	12.5	116.5	24.0	89.6	63.4	5044.6

Table A3.7. $L_C/D = 20$, $L_H/D = 20$.

Test No.	T_H (°C)	T_C (°C)	$T_H - T_C$ (°C)	T_{ROOM} (°C)	Q_G (W)	Q_N (W)	\dot{q} (W/m ²)
1	39.4	12.0	27.4	23.5	26.1	21.3	852.0
2	50.0	12.0	48.0	23.5	73.5	65.6	2625.0
3	65.6	12.0	53.6	23.5	138.8	129.2	5168.0
4	74.4	12.0	62.4	23.5	216.3	201.0	8040.0
5	82.5	12.0	70.5	23.5	321.0	303.3	12132.0
6	92.5	12.5	80.0	23.5	442.1	421.4	16856.0
7	107.7	13.0	94.7	23.5	633.8	608.5	24340.0

Table A3.8. $L_C/D = 20$, $L_H/D = 40$.

Test No.	T_H (°C)	T_C (°C)	$T_H - T_C$ (°C)	T_{ROOM} (°C)	Q_G (W)	Q_N (W)	\dot{q} (W/m ²)
1	37.3	10.0	27.3	24.0	47.0	42.0	840.0
2	40.2	10.2	30.0	24.0	160.2	154.0	3080.0
3	58.2	10.4	47.8	24.0	331.3	318.3	6366.0
4	65.6	11.1	54.5	24.0	503.6	487.8	9756.0
5	75.5	12.0	63.5	24.0	765.8	746.0	14920.0
6	88.5	13.0	75.5	24.0	1127.7	1103.2	22064.0
7	100.2	18.0	82.2	24.0	1524.7	1495.7	29914.0
8	111.0	20.5	90.5	24.0	1826.0	1792.9	35858.0

Table A3.9. $L_H/D = 20$, $L_C/D = 10$.

Test No.	T_H (°C)	T_C (°C)	$T_H - T_C$ (°C)	T_{ROOM} (°C)	Q_G (W)	Q_N (W)	\dot{q} (W/m ²)
1	53.1	19.0	34.1	23.0	30.3	21.3	852.0
2	57.7	19.0	38.7	23.0	76.2	65.8	2632.0
3	72.5	19.0	53.5	23.0	158.6	143.8	5750.0
4	80.2	19.0	61.2	23.0	243.3	226.1	9044.0
5	89.3	19.3	70.0	23.0	367.9	348.0	13920.0
6	102.2	20.5	81.7	23.0	527.3	503.5	20140.0
7	116.8	19.5	97.3	23.0	732.0	703.9	28156.0
8	133.0	19.5	113.5	23.0	920.4	887.4	35496.0

Table A3.10. $L_H/D = 20$, $L_C/D = 40$.

Test No.	T_H (°C)	T_C (°C)	$T_H - T_C$ (°C)	T_{ROOM} (°C)	Q_G (W)	Q_N (W)	\dot{q} (W/m ²)
1	34.8	14.0	20.8	24.0	24.8	20.4	817.1
2	48.4	13.5	34.9	24.0	79.2	71.9	2876.5
3	60.4	14.0	46.4	24.0	155.3	144.4	5776.9
4	68.0	14.0	54.0	24.0	250.4	237.2	9507.3
5	77.0	14.0	63.0	24.0	349.1	333.2	13329.6
6	86.4	14.0	72.4	24.0	450.2	431.5	17260.0
7	97.6	14.0	83.6	24.0	592.0	575.9	23036.0
8	113.4	14.2	99.2	24.0	814.9	788.1	31524.0

Table A3.11. $L_H/D = L_C/D = 10$.

Test No.	T_H (°C)	T_C (°C)	$T_H - T_C$ (°C)	T_{ROOM} (°C)	Q_G (W)	Q_N (W)	\dot{q} (W/m ²)
1	34.6	14.6	20.0	22.0	15.1	11.9	943.6
2	58.5	14.5	44.0	22.0	37.1	28.0	2228.2
3	90.7	14.5	76.2	22.0	81.5	64.3	5116.8
4	120.8	14.8	106.0	22.0	106.4	81.7	6501.5

Table A3.12. $L_H/D = L_C/D = 30$.

Test No.	T_H (°C)	T_C (°C)	$T_H - T_C$ (°C)	T_{ROOM} (°C)	Q_G (W)	Q_N (W)	\dot{q} (W/m ²)
1	44.4	12.4	32.0	24.0	45.4	38.5	1021.8
2	58.8	12.5	46.3	24.0	202.0	188.8	5008.0
3	69.5	12.5	57.0	24.0	442.7	427.2	11332.0
4	79.7	12.5	67.2	24.0	713.4	694.5	18423.4
5	89.1	12.6	76.5	24.0	888.7	866.6	22987.5
6	96.4	12.6	83.8	24.0	1146.4	1121.8	29758.0
7	107.0	13.0	94.0	24.0	1360.2	1332.0	35332.8

Table A3.13. $L_H/D = L_C/D = 40$.

Test No.	T_H (°C)	T_C (°C)	$T_H - T_C$ (°C)	T_{ROOM} (°C)	Q_G (W)	Q_N (W)	\dot{q} (W/m ²)
1	44.8	10.7	34.1	24.0	54.8	46.9	933.0
2	50.0	11.0	39.0	24.0	254.4	244.5	4867.0
3	60.2	13.0	47.2	24.0	552.3	538.5	10717.0
4	73.8	17.8	56.0	24.0	944.9	926.0	18428.0
5	85.0	19.2	65.8	24.0	1305.0	1281.8	25508.8
6	99.0	20.3	78.7	24.0	1703.4	1674.9	33330.3
7	110.0	21.3	88.7	24.0	2061.0	2028.3	40363.6

3. Experiments of Tube Orientation

Table A3.14. $\phi_r = 0^\circ$, $\phi_t = 0^\circ$.

Test No.	T_H (°C)	T_C (°C)	$T_H - T_C$ (°C)	T_{ROOM} (°C)	Q_G (W)	Q_N (W)	\dot{q} (W/m ²)
1	40.3	17.0	23.3	26.0	14.7	10.4	416.0
2	54.7	17.0	37.7	26.0	50.5	41.9	1676.0
3	59.0	17.5	41.5	26.0	112.5	102.6	4104.0
4	66.7	19.2	47.5	26.0	182.7	170.5	6820.0
5	78.0	20.0	58.0	26.0	339.4	323.8	12952.0
6	89.8	19.0	79.8	26.0	515.0	495.9	19836.0
7	109.4	19.5	89.9	26.0	766.3	741.3	29652.0

Table A3.15. $\phi_r = 0^\circ$, $\phi_i = 3^\circ$.

Test No.	T_H (°C)	T_C (°C)	$T_H - T_C$ (°C)	T_{ROOM} (°C)	Q_G (W)	Q_N (W)	\dot{q} (W/m ²)
1	38.2	19.0	19.2	24.5	.3	12.2	488.0
2	45.5	19.0	26.5	24.5	48.8	42.5	1700.0
3	56.5	19.6	36.9	24.5	113.6	104.0	4160.0
4	64.3	19.7	44.64	24.5	197.7	185.8	7432.0
5	74.4	20.6	53.8	24.5	326.0	311.0	12440.0
6	86.4	20.3	66.1	24.5	490.4	471.8	18871.5
7	100.5	23.0	77.5	24.5	667.2	644.4	25777.0
8	116.0	23.0	93.0	24.5	856.8	829.4	33176.0

Table A3.16. $\phi_r = 0^\circ$, $\phi_i = 6^\circ$.

Test No.	T_H (°C)	T_C (°C)	$T_H - T_C$ (°C)	T_{ROOM} (°C)	Q_G (W)	Q_N (W)	\dot{q} (W/m ²)
1	35.2	20.8	14.4	26.0	15.1	12.3	492.0
2	58.0	21.5	36.5	26.0	33.4	23.8	952.0
3	64.5	21.5	43.0	26.0	123.4	111.9	4476.0
4	72.1	21.7	50.4	26.0	219.4	205.6	8224.0
5	80.9	22.6	58.3	26.0	345.2	328.7	13148.0
6	90.1	22.8	67.3	26.0	494.8	475.6	19024.0
7	102.3	25.0	77.3	26.0	687.9	665.0	26600.0

Table A3.17. $\phi_r = 0^\circ$, $\phi_t = 13^\circ$.

Test No.	T_H (°C)	T_C (°C)	$T_H - T_C$ (°C)	T_{ROOM} (°C)	Q_G (W)	Q_N (W)	\dot{q} (W/m ²)
1	49.3	20.8	28.5	25.5	50.7	43.6	1744.0
2	52.7	21.0	31.5	25.5	114.5	106.3	4252.0
3	60.5	21.5	39.0	25.5	217.1	206.6	8264.0
4	70.0	22.0	48.0	25.5	346.5	333.2	13326.0
5	81.3	22.5	58.8	25.5	520.5	503.8	20152.0
6	94.0	23.5	70.5	25.5	688.5	668.0	26720.0
7	110.5	25.0	85.5	25.5	923.5	898.0	35922.0

Table A3.18. $\phi_r = 0^\circ$, $\phi_t = 15^\circ$.

Test No.	T_H (°C)	T_C (°C)	$T_H - T_C$ (°C)	T_{ROOM} (°C)	Q_G (W)	Q_N (W)	\dot{q} (W/m ²)
1	43.5	17.2	26.3	25.0	53.1	47.5	1900.0
2	48.3	17.2	31.1	25.0	123.6	116.6	4664.0
3	56.5	17.5	39.0	25.0	235.3	225.9	9036.0
4	67.0	19.0	48.0	25.0	402.8	390.2	15608.0
5	81.0	20.5	60.5	25.0	586.1	569.3	22772.0

Table A3.19. $\phi_r = 0^\circ$, $\phi_i = 30^\circ$.

Test No.	T_H (°C)	T_C (°C)	$T_H - T_C$ (°C)	T_{ROOM} (°C)	Q_G (W)	Q_N (W)	\dot{q} (W/m ²)
1	51.1	21.0	30.1	25.0	50.8	43.0	1720.0
2	57.0	21.0	36.0	25.0	123.9	114.3	4572.0
3	66.0	21.0	45.0	25.0	222.1	209.8	8392.0
4	75.5	21.5	54.0	25.0	359.4	344.2	13768.0
5	85.0	22.5	62.5	25.0	514.4	496.4	19856.0
6	97.7	23.0	74.7	25.0	691.6	669.8	26792.0
7	107.2	24.0	83.2	25.0	838.9	814.2	32568.0

Table A3.20. $\phi_r = 0^\circ$, $\phi_i = 60^\circ$.

Test No.	T_H (°C)	T_C (°C)	$T_H - T_C$ (°C)	T_{ROOM} (°C)	Q_G (W)	Q_N (W)	\dot{q} (W/m ²)
1	43.3	17.2	26.1	25.0	51.5	46.0	1840.0
2	48.9	17.2	31.7	25.0	118.3	111.1	4444.0
3	56.8	18.7	38.1	25.0	223.3	213.8	8552.0
4	65.2	19.6	45.6	25.0	351.4	339.3	13572.0
5	76.4	20.3	56.1	25.0	507.8	492.4	19696.0
6	90.0	21.8	68.2	25.0	698.6	679.1	27164.0
7	107.0	22.5	84.5	25.0	918.9	894.3	35772.0

Table A3.21. $\phi_r = 0^\circ$, $\phi_t = 80^\circ$.

Test No.	T_H (°C)	T_C (°C)	$T_H - T_C$ (°C)	T_{ROOM} (°C)	Q_G (W)	Q_N (W)	\dot{q} (W/m ²)
1	45.7	18.5	27.2	25.0	56.9	50.7	2028.0
2	60.2	18.5	41.7	25.0	145.0	134.4	5376.0
3	68.5	19.0	49.5	25.0	264.7	251.7	10068.0
4	77.0	20.0	57.0	25.0	396.2	380.6	15224.0
5	90.5	21.0	69.5	25.0	585.8	566.1	22644.0
6	105.0	21.2	83.8	25.0	787.2	763.2	30528.0

Table A3.22. $\phi_r = 0^\circ$, $\phi_t = 87^\circ$.

Test No.	T_H (°C)	T_C (°C)	$T_H - T_C$ (°C)	T_{ROOM} (°C)	Q_G (W)	Q_N (W)	\dot{q} (W/m ²)
1	43.6	18.5	25.1	25.0	61.9	56.3	2252.0
2	49.7	19.0	30.7	25.0	141.1	133.7	5348.0
3	57.1	20.0	37.1	25.0	252.0	242.4	9696.0
4	68.5	21.0	47.5	25.0	410.6	397.6	15904.0
5	82.9	22.0	60.9	25.0	620.6	603.2	24128.0
6	100.0	23.0	77.0	25.0	821.9	799.4	31976.0

Table A3.23. $\phi_r = 0^\circ$, $\phi_t = 90^\circ$.

Test No.	T_H (°C)	T_C (°C)	$T_H - T_C$ (°C)	T_{ROOM} (°C)	Q_G (W)	Q_N (W)	\dot{q} (W/m ²)
1	51.0	18.3	32.7	24.0	42.8	34.7	1388.0
2	62.5	18.3	44.2	24.0	109.3	97.8	3912.0
3	75.3	19.0	56.3	24.0	224.9	209.5	8380.0
4	87.7	19.5	68.2	24.0	368.7	349.6	13984.0
5	100.0	20.0	80.0	24.0	529.8	507.0	20280.0
6	113.6	21.0	92.6	24.0	663.5	636.6	25464.0

Table A3.24. $\phi_r = 30^\circ$, $\phi_t = 3^\circ$.

Test No.	T_H (°C)	T_C (°C)	$T_H - T_C$ (°C)	T_{ROOM} (°C)	Q_G (W)	Q_N (W)	\dot{q} (W/m ²)
1	40.0	20.0	20.0	28.0	15.7	12.1	484.0
2	53.1	20.0	33.1	28.0	54.0	46.5	1860.0
3	59.2	20.4	38.8	28.0	112.5	103.1	4124.0
4	66.4	20.0	46.4	28.0	228.2	216.7	8668.0
5	74.0	21.0	53.0	28.0	333.1	319.3	12772.0
6	80.8	23.0	57.8	28.0	484.1	468.3	18732.0
7	100.5	23.0	77.5	28.0	667.4	645.6	25824.0
8	116.5	25.0	91.5	28.0	865.8	839.3	33572.0

Table A3.25. $\phi_r = 30^\circ$, $\phi_t = 15^\circ$.

Test No.	T_H (°C)	T_C (°C)	$T_H - T_C$ (°C)	T_{ROOM} (°C)	Q_G (W)	Q_N (W)	\dot{q} (W/m ²)
1	59.0	17.5	42.5	24.0	138.4	127.9	5116.0
2	71.0	18.0	53.0	24.0	261.0	246.9	9876.0
3	87.5	19.5	68.0	24.0	453.5	434.4	17376.0
4	104.0	20.5	83.5	24.0	682.5	658.5	26340.0
5	120.0	22.0	98.0	24.0	905.0	876.2	35048.0

Table A3.26. $\phi_r = 30^\circ$, $\phi_t = 30^\circ$.

Test No.	T_H (°C)	T_C (°C)	$T_H - T_C$ (°C)	T_{ROOM} (°C)	Q_G (W)	Q_N (W)	\dot{q} (W/m ²)
1	51.0	21.0	30.0	26.0	52.3	44.8	1792.0
2	70.3	21.0	49.3	26.0	154.6	141.3	5652.0
3	76.5	21.0	55.5	26.0	273.4	258.2	10328.0
4	87.0	22.0	65.0	26.0	446.9	428.6	17144.0
5	98.5	23.0	75.5	26.0	619.5	597.7	23908.0
6	111.5	24.0	87.5	26.0	820.7	795.1	31804.0
7	121.5	25.0	96.5	26.0	965.2	936.6	37464.0

Table A3.27. $\phi_r = 30^\circ$, $\phi_t = 80^\circ$.

Test No.	T_H (°C)	T_C (°C)	$T_H - T_C$ (°C)	T_{ROOM} (°C)	Q_G (W)	Q_N (W)	\dot{q} (W/m ²)
1	71.6	22.0	49.6	24.5	403.6	389.5	15580.0
2	90.5	24.0	66.5	24.5	700.0	680.3	27212.0
3	106.0	25.5	80.5	24.5	920.0	895.6	35824.0

Table A3.28. $\phi_r = 30^\circ$, $\phi_t = 90^\circ$.

Test No.	T_H (°C)	T_C (°C)	$T_H - T_C$ (°C)	T_{ROOM} (°C)	Q_G (W)	Q_N (W)	\dot{q} (W/m ²)
1	48.8	17.8	31.0	23.5	53.0	45.4	1816.0
2	66.3	17.8	48.5	23.5	126.8	114.0	4560.0
3	74.5	18.5	56.0	23.5	227.3	212.0	8480.0
4	84.0	19.5	64.5	23.5	361.0	342.9	13716.0
5	100.0	21.0	79.0	23.5	556.0	533.0	21320.0
6	113.0	22.0	91.0	23.5	720.3	693.5	27740.0

Table A3.29. $\phi_r = 45^\circ$, $\phi_t = 15^\circ$.

Test No.	T_H (°C)	T_C (°C)	$T_H - T_C$ (°C)	T_{ROOM} (°C)	Q_G (W)	Q_N (W)	\dot{q} (W/m ²)
1	44.5	17.5	27.0	24.0	54.5	48.3	1932.0
2	61.3	17.8	43.5	24.0	147.7	136.5	5460.0
3	74.3	18.7	55.6	24.0	258.6	243.5	9740.0
4	84.3	19.0	65.3	24.0	391.1	373.0	14920.0
5	97.0	19.5	77.5	24.0	591.2	569.3	22772.0
6	109.0	20.0	89.0	24.0	751.8	726.3	29052.0

Table A3.30. $\phi_r = 45^\circ$, $\phi_t = 30^\circ$.

Test No.	T_H (°C)	T_C (°C)	$T_H - T_C$ (°C)	T_{ROOM} (°C)	Q_G (W)	Q_N (W)	\dot{q} (W/m ²)
1	54.0	21.0	33.0	26.0	149.3	140.9	5636.0
2	63.3	21.0	42.3	26.0	290.2	279.0	11160.0
3	75.0	21.5	53.5	26.0	458.7	444.0	17760.0
4	88.0	22.0	66.0	26.0	654.8	636.2	25448.0
5	101.7	23.0	78.7	26.0	847.4	824.7	32988.0
6	111.5	23.5	88.0	26.0	983.4	957.7	38308.0

Table A3.31. $\phi_r = 45^\circ$, $\phi_t = 60^\circ$.

Test No.	T_H (°C)	T_C (°C)	$T_H - T_C$ (°C)	T_{ROOM} (°C)	Q_G (W)	Q_N (W)	\dot{q} (W/m ²)
1	47.2	18.0	29.2	24.0	62.0	55.0	2200.0
2	54.3	18.0	36.3	24.0	138.7	129.6	5184.0
3	64.6	18.5	46.1	24.0	254.9	242.7	9708.0
4	75.0	19.5	55.5	24.0	391.6	376.3	15052.0
5	88.0	21.0	67.0	24.0	553.2	534.0	21360.0
6	100.2	22.0	78.2	24.0	742.1	719.2	28768.0
7	115.0	23.0	92.0	24.0	947.0	919.7	36788.0

Table A3.32. $\phi_r = 45^\circ$, $\phi_t = 80^\circ$.

Test No.	T_H (°C)	T_C (°C)	$T_H - T_C$ (°C)	T_{ROOM} (°C)	Q_G (W)	Q_N (W)	\dot{q} (W/m ²)
1	50.0	21.0	29.0	24.5	140.5	132.9	5316.0
2	59.0	21.0	38.0	24.5	262.3	252.0	10080.0
3	71.0	22.0	49.0	24.5	432.0	418.0	16720.0
4	86.5	23.0	62.5	24.5	644.6	626.0	25040.0
5	98.0	24.0	74.0	24.5	803.4	781.4	31256.0
6	110.0	25.0	85.0	24.5	967.2	941.5	37660.0

Table A3.33. $\phi_r = 45^\circ$, $\phi_t = 90^\circ$.

Test No.	T_H (°C)	T_C (°C)	$T_H - T_C$ (°C)	T_{ROOM} (°C)	Q_G (W)	Q_N (W)	\dot{q} (W/m ²)
1	47.5	18.0	29.5	23.8	53.3	46.2	1848.0
2	58.6	18.0	40.6	23.8	133.8	123.4	4936.0
3	70.2	18.5	51.7	23.8	241.2	227.3	9092.0
4	79.7	19.5	60.2	23.8	375.1	358.3	14332.0
5	91.3	21.0	70.3	23.8	543.3	523.1	20924.0
6	107.4	22.0	85.4	23.8	727.3	702.2	28088.0

Table A3.34. $\phi_r = 60^\circ$, $\phi_t = 30^\circ$.

Test No.	T_H (°C)	T_C (°C)	$T_H - T_C$ (°C)	T_{ROOM} (°C)	Q_G (W)	Q_N (W)	\dot{q} (W/m ²)
1	57.5	21.5	36.0	25.0	146.8	137.0	5480.0
2	65.8	22.0	43.8	25.0	270.6	258.4	10336.0
3	78.5	22.5	56.0	25.0	470.6	454.5	18180.0
4	88.5	23.5	65.0	25.0	677.5	658.4	26336.0
5	113.5	24.0	89.5	25.0	942.0	915.4	36616.0

Table A3.35. $\phi_r = 60^\circ$, $\phi_i = 60^\circ$.

Test No.	T_H (°C)	T_C (°C)	$T_H - T_C$ (°C)	T_{ROOM} (°C)	Q_G (W)	Q_N (W)	\dot{q} (W/m ²)
1	51.8	17.8	34.0	23.5	58.3	49.8	1992.0
2	62.1	17.8	44.3	23.5	137.6	126.0	5040.0
3	79.7	18.3	61.4	23.5	261.6	244.7	9788.0
4	94.5	19.0	75.5	23.5	405.2	383.9	15356.0
5	106.0	20.0	86.0	23.5	587.8	563.0	22520.0
6	118.0	21.0	97.0	23.5	790.3	762.0	30480.0

Table A3.36. $\phi_r = 60^\circ$, $\phi_i = 80^\circ$.

Test No.	T_H (°C)	T_C (°C)	$T_H - T_C$ (°C)	T_{ROOM} (°C)	Q_G (W)	Q_N (W)	\dot{q} (W/m ²)
1	57.7	21.0	36.7	24.5	152.5	142.5	5700.0
2	66.5	21.5	45.0	24.5	288.4	275.8	11032.0
3	78.3	22.0	56.3	24.5	462.6	446.5	17860.0
4	93.8	23.0	70.8	24.5	671.8	651.0	26040.0
5	110.0	24.0	86.0	24.5	899.7	874.0	34960.0

Table A3.37. $\phi_r = 60^\circ$, $\phi_t = 90^\circ$.

Test No.	T_H (°C)	T_C (°C)	$T_H - T_C$ (°C)	T_{ROOM} (°C)	Q_G (W)	Q_N (W)	\dot{q} (W/m ²)
1	46.0	17.3	28.7	24.0	48.1	41.5	1660.0
2	49.7	17.5	32.2	24.0	123.5	115.8	4632.0
3	56.2	18.5	37.7	24.0	237.0	227.4	9096.0
4	70.0	19.0	51.0	24.0	406.0	392.3	15692.0
5	85.8	20.0	65.8	24.0	568.5	550.0	22000.0

Table A3.38. $\phi_r = 80^\circ$, $\phi_t = 90^\circ$.

Test No.	T_H (°C)	T_C (°C)	$T_H - T_C$ (°C)	T_{ROOM} (°C)	Q_G (W)	Q_N (W)	\dot{q} (W/m ²)
1	52.0	18.0	34.0	23.5	61.6	53.1	2124.0
2	56.7	18.0	48.7	23.5	135.6	122.6	4904.0
3	74.3	18.5	55.8	23.5	245.4	230.2	9208.0
4	87.0	19.5	67.5	23.5	379.8	360.8	14432.0
5	98.5	21.0	77.5	23.5	541.2	518.7	20748.0
6	113.0	22.0	91.0	23.5	729.2	702.3	28092.0

Table A3.39. $\phi_r = 90^\circ$, $\phi_i = 15^\circ$.

Test No.	T_H (°C)	T_C (°C)	$T_H - T_C$ (°C)	T_{ROOM} (°C)	Q_G (W)	Q_N (W)	\dot{q} (W/m ²)
1	55.4	18.0	37.4	23.5	57.2	47.6	1904.0
2	66.5	18.5	48.0	23.5	138.9	126.0	5040.0
3	79.7	19.5	60.2	23.5	243.7	226.8	9072.0
4	88.0	21.0	67.0	23.5	386.8	367.5	14700.0
5	100.5	22.0	78.5	23.0	561.8	538.7	21548.0
6	115.0	23.0	92.0	23.5	773.0	745.5	29820.0
7	122.0	23.0	99.0	23.5	866.7	837.1	33484.0

Table A3.40. $\phi_r = 90^\circ$, $\phi_i = 30^\circ$.

Test No.	T_H (°C)	T_C (°C)	$T_H - T_C$ (°C)	T_{ROOM} (°C)	Q_G (W)	Q_N (W)	\dot{q} (W/m ²)
1	55.0	21.2	33.8	25.0	61.7	52.7	2108.0
2	69.0	21.2	47.8	25.0	175.0	161.8	6472.0
3	83.0	22.0	61.0	25.0	323.1	305.7	12228.0
4	97.0	23.0	74.0	25.0	510.6	489.0	19560.0
5	112.0	24.5	87.5	25.0	697.0	671.0	26840.0
6	124.0	25.0	99.0	25.0	879.1	849.4	33976.0

Table A3.41. $\phi_r = 90^\circ$, $\phi_t = 60^\circ$.

Test No.	T_H (°C)	T_C (°C)	$T_H - T_C$ (°C)	T_{ROOM} (°C)	Q_G (W)	Q_N (W)	\dot{q} (W/m ²)
1	41.3	18.0	23.3	24.0	54.5	49.3	1972.0
2	47.0	18.0	29.0	24.0	134.7	127.8	5112.0
3	55.9	18.5	37.4	24.0	254.3	244.7	9788.0
4	66.4	19.0	47.4	24.0	399.8	387.1	15484.0
5	79.7	20.0	59.7	24.0	588.9	572.2	22888.0
6	93.7	21.0	72.7	24.0	801.8	780.9	31236.0
7	107.0	23.0	84.0	24.0	962.4	937.5	37500.0

Table A3.42. $\phi_r = 90^\circ$, $\phi_t = 90^\circ$.

Test No.	T_H (°C)	T_C (°C)	$T_H - T_C$ (°C)	T_{ROOM} (°C)	Q_G (W)	Q_N (W)	\dot{q} (W/m ²)
1	49.1	16.5	32.6	24.0	44.6	37.1	1484.0
2	95.0	17.0	78.0	24.0	137.6	116.3	2660.0

APPENDIX 4

ESTIMATED UNCERTAINTY

The estimated uncertainties associated with the experimental measurements and calculated experimental results are briefly discussed in this section.

The uncertainties in the filling charge (v_p) and the angles of inclination (ϕ) were both small, being less than ± 2 ml and $\pm 0.1^\circ$, respectively. The uncertainties in the dimensions (diameter and length) were ± 0.001 cm and ± 0.1 cm, respectively. The manufacturer of the voltmeter and ammeter used in the present study states that the voltmeter accuracy is ± 0.1 V and the ammeter accuracy is ± 0.01 A. The uncertainty of the thermocouple measurements was ± 0.5 °C, but due to the temperature fluctuation at some points in the system, the temperature uncertainties for stable points and unstable points were chosen at ± 0.5 °C and ± 1.5 °C, respectively. Following the technique recommended in the notes of MEC E 400⁵ and assuming the above uncertainties have normal distributions, they were combined to yield a maximum $\pm 1.5\%$ uncertainty in the heat flux density.

The following is an example of the uncertainty calculation.

- (1) the results of the measurements are

⁵ MEC E 400, Statistical Analysis of Data, Department of Mechanical Engineering, University of Alberta, 1987.

$$T_H = 69 \pm 1.5 \text{ }^\circ\text{C}, \quad T_C = 32.5 \pm 0.5 \text{ }^\circ\text{C},$$

$$\Delta T = 37.5 \text{ }^\circ\text{C}$$

$$V_1 = 46.1 \pm 0.1 \text{ V}, \quad V_2 = 44.9 \pm 0.1 \text{ V},$$

$$I_1 = 3.61 \pm 0.01 \text{ A}, \quad I_2 = 3.81 \pm 0.01 \text{ A},$$

$$L_H = L_C = 40.0 \pm 0.1 \text{ cm}, \quad D = 2.000 \pm 0.001 \text{ cm},$$

(2) the uncertainty of temperature difference is that

$$\begin{aligned} \varepsilon_{\Delta T} &= (\varepsilon_{T_H}^2 + \varepsilon_{T_C}^2)^{\frac{1}{2}} \\ &= (1.5^2 + 0.5^2)^{\frac{1}{2}} \\ &= 1.6 \text{ }^\circ\text{C} \end{aligned}$$

thus $\Delta T = 37.5 \pm 1.6 \text{ }^\circ\text{C}$

(3) the uncertainty of the gross heat flux:

$$\begin{aligned} \varepsilon_{Q_o} &= [(I_1^2 + I_2^2) \varepsilon_{V_1}^2 + (V_1^2 + V_2^2) \varepsilon_{I_1}^2]^{\frac{1}{2}} \\ &= [(3.61^2 + 3.81^2) \times 0.1^2 + (46.1^2 \\ &\quad + 44.9^2) \times 0.01^2]^{\frac{1}{2}} \\ &= 0.8 \text{ W} \end{aligned}$$

assuming that the uncertainty of the heat loss is 0.5 W thus the uncertainty of the net heat flux is given by

$$\begin{aligned}
 \varepsilon_{Q_n} &= (\varepsilon_{Q_o}^2 + \varepsilon_{Q_i}^2)^{\frac{1}{2}} \\
 &= (0.8^2 + 0.5^2)^{\frac{1}{2}} \\
 &= 0.9 \text{ W}
 \end{aligned}$$

(4) the heat flux density is

$$\begin{aligned}
 \dot{q} &= \frac{Q_N}{A} = \frac{Q_N}{\left(\pi D L_H + \frac{\pi D^2}{4}\right)} \\
 &= 13 \text{ kW/m}^2
 \end{aligned}$$

and the uncertainty of the heat flux density is

$$\begin{aligned}
 \varepsilon_{\dot{q}} &= \left\{ \left[\left(\frac{\varepsilon_{Q_N}}{Q_N}\right)^2 + \left(\frac{\varepsilon_{L_H}}{L_H}\right)^2 + 5 \left(\frac{\varepsilon_D}{D}\right)^2 \right] \dot{q}^2 \right\}^{\frac{1}{2}} \\
 &= 0.05 \text{ kW/m}^2
 \end{aligned}$$

hence $\dot{q} = 13 \pm 0.05 \text{ kW/m}^2$.

APPENDIX 5

EMPIRICAL CORRELATION

The following analysis is based on the data obtained in chapter 3; a horizontal condenser lies above a vertical evaporator.

In general, the Nusselt number is a function of the identified parameters. From the experiment,

$$Nu_D = f\left(v_R, \frac{L_H}{D}, \frac{L_C}{D}, \Phi\right) \quad (\text{A5.1})$$

where Φ is a dimensionless function of temperature difference, $T_H - T_C$, between evaporator and condenser.

To obtain the expression Φ , first consider that the heat flux density

$$\dot{q} \sim \frac{\phi^n}{(1 + c \phi^n)}$$

and

$$\phi = \frac{T_H - T_C}{\Delta T_f}$$

where ΔT_f is an arbitrary reference temperature difference. In this case, ΔT_f has been chosen as 50 K to represent the division between low ΔT data ($\Delta T < 50$ K) and high ΔT data ($\Delta T > 50$ K). We now seek a power law relation

$$Nu_D = B v_R^{m_1} \left(\frac{L_H}{D}\right)^{m_2} \left(\frac{L_C}{D}\right)^{m_3} \frac{\phi^{n-1}}{(1 + c \phi^n)} \quad (\text{A5.2})$$

Replotting the data in chapter 3, we find that

$$m_1 = 1.57 \pm 0.15,$$

$$m_2 = 0.41 \pm 0.05,$$

$$m_3 = 0.144 \pm 0.05,$$

$$n = 2.72 \pm 0.4,$$

$$B = 3.9 \pm 0.1,$$

and

$$c = 0.063 \pm 0.005$$

for the experimental ranges

$$30\% \leq v_R \leq 50\%,$$

$$20 \leq L_H/D \leq 40,$$

$$10 \leq L_C/D \leq 40,$$

and

$$20 \leq T_H - T_C \leq 100.$$

Hence

$$Nu_D = 3.9 v_R^{1.57} \left(\frac{L_H}{D}\right)^{0.41} \left(\frac{L_C}{D}\right)^{0.144} \frac{\phi^{1.72}}{(1 + 0.063 \phi^{2.72})} \quad (\text{A5.3})$$

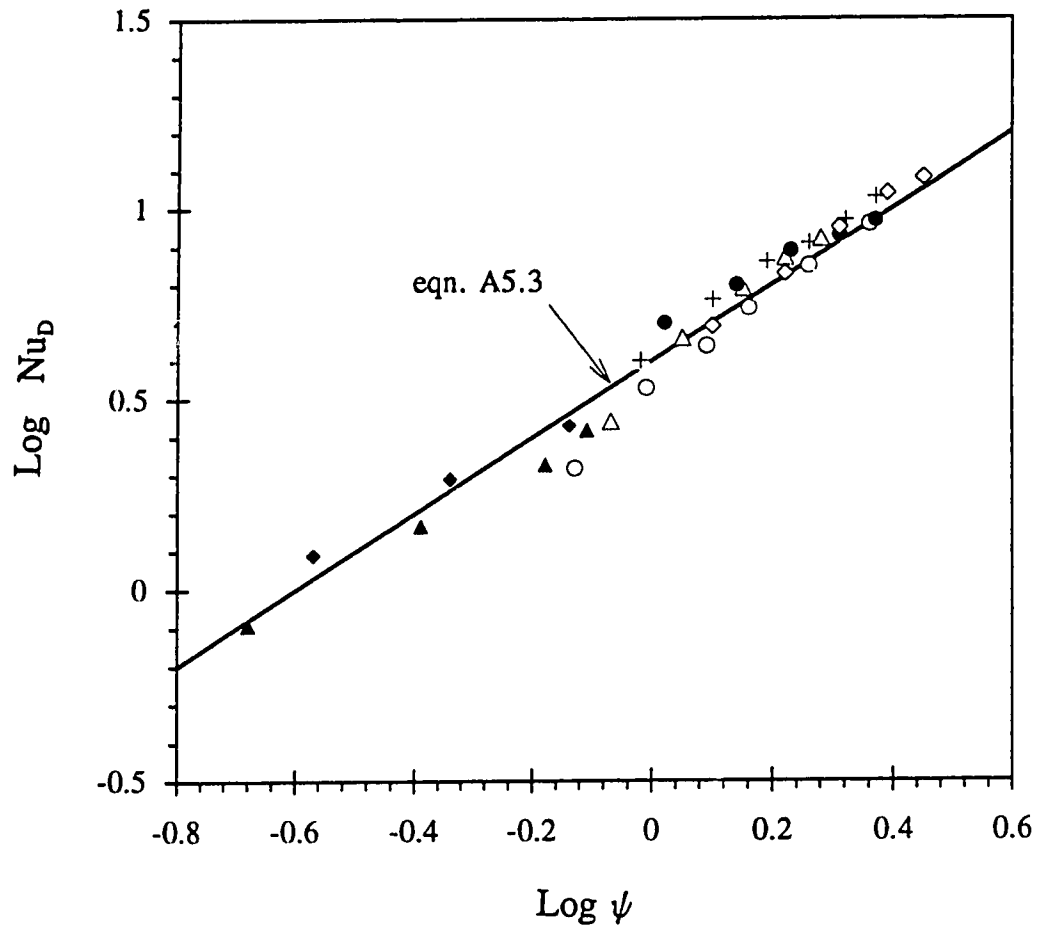
Fig. A5.1 shows this result together with the experimental data. where

$$\psi = v_R^{1.57} \left(\frac{L_H}{D}\right)^{0.41} \left(\frac{L_C}{D}\right)^{0.144} \frac{\phi^{1.72}}{(1 + 0.063 \phi^{2.72})}$$

Most of the experimental results agree with the correlation to within $\pm 15\%$ over the range considered except that three points agree with it to within -30% perhaps because

of the larger uncertainties on the heat losses.

Eqn. A5.3 gives the designer useful information in the performance range, or design state. A comparison is also given in fig. A5.2 to the performance beyond this range, or off-design state.



Data ranges:

$$30\% \leq v_R \leq 50\%;$$

$$20 \leq L_H/D \leq 40;$$

$$20 \leq T_H - T_C \leq 100;$$

$$10 \leq L_C/D \leq 40;$$

Fig. A5.1 Comparison of empirical correlation with design-state results.

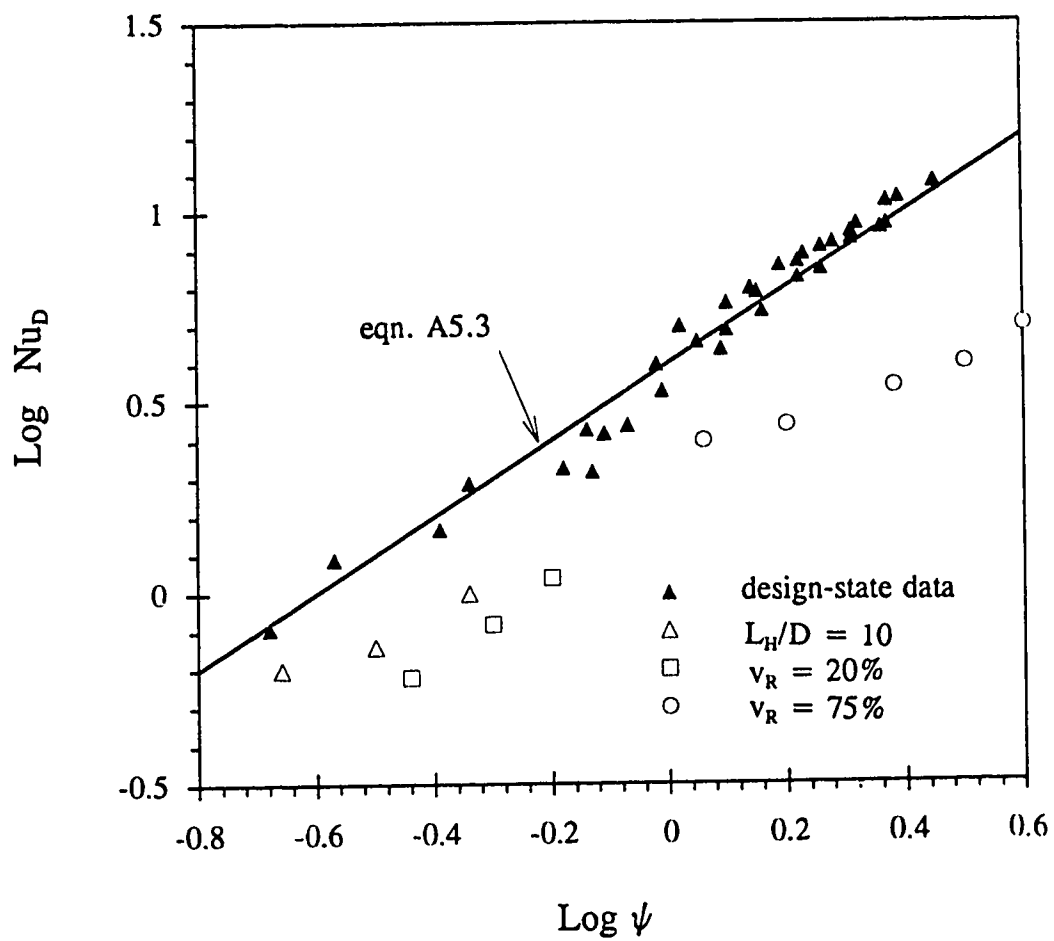


Fig. A5.2 Comparison of empirical correlation with off-design results.

APPENDIX 6

FLOW VISUALIZATION

In chapter 3 and 4, it was mentioned that a set of simulating experiments was undertaken by assuming $\dot{q}A_H \approx \dot{m}\lambda$. In this section, the flow visualization apparatus and some photographs are given to support the explanations of hydrodynamic behaviour in the thermosyphon. Fig. A6.1 shows the schematic of the apparatus. Fig. A6.2 to Fig. A6.8 refer to the flow behaviour of the thermosyphon at various working conditions, as indicated at each figure. The shutter speeds of the photographs were 1/500 second. The film of the photographs was Kodak TMAX E.I. 400/27'. Two 500 watt bulbs in reflectors set at 45 degrees to illuminate grey background providing indirect lighting on the tube. The pins attached to the tube give the length scale on the evaporator and condenser. The interval between the pins is 4 cm, i.e. 2 diameters.

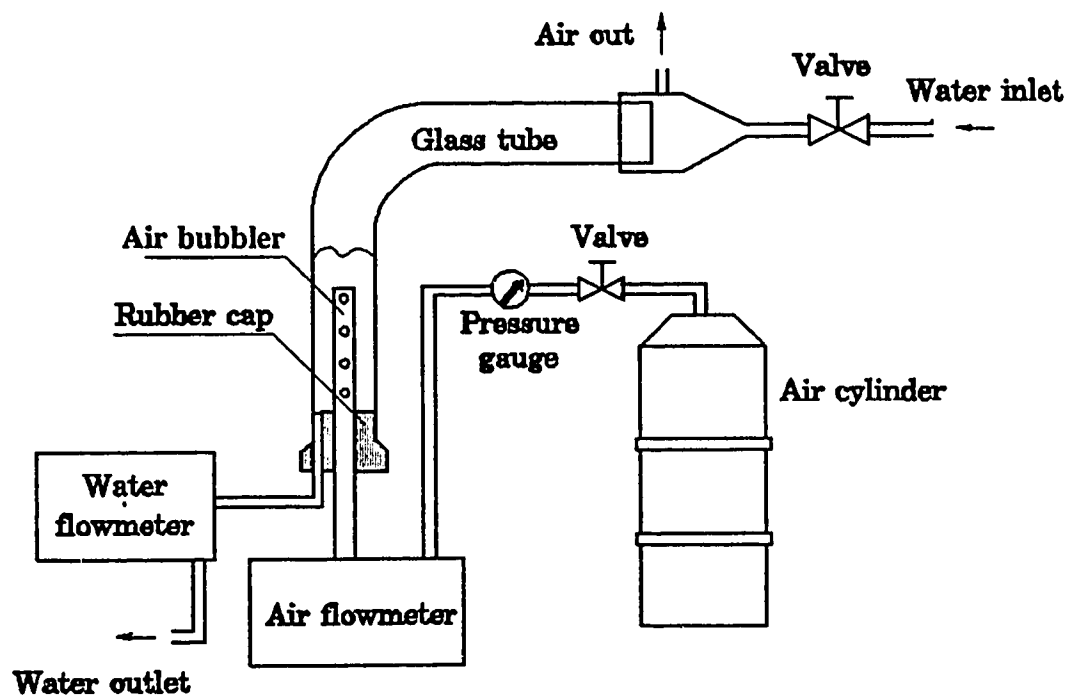


Fig. A6.1 Schematic of flow visualization.

Figures A6.3 & A6.4² have been removed
due to poor print quality

refer to Fig. 2.5 and page 20.
 $\dot{q} = 25 \text{ kW/m}^2$, $\dot{m} = 1.13 \text{ kg/hr}$.

Fig. A6.2 **Flooding phenomenon in
horizontal condenser.**

refer to Fig. 3.4 and page 36.
 $L_H/D = 10$, $\dot{q} = 5 \text{ kW/m}^2$
 $\dot{m} = 0.113 \text{ kg/hr}$.

Fig. A6.3 **Dry surface at the upper section
of a vertical evaporator.**

Figures A6.4 & A6.5 have been removed due to poor print quality.

refer to Fig. 3.4 and page 37.
 $\dot{q} = 25 \text{ kW/m}^2$, $\dot{m} = 1.13 \text{ kg/hr}$.

Fig. A6.4 **Plug flow and bubbly flow in a vertical evaporator.**

refer to Fig 4.3 and page 53.
 $\phi_t = 30^\circ$, $\phi_r = 90^\circ$
 $\dot{q} = 20 \text{ kW/m}^2$, $\dot{m} = 0.91 \text{ kg/hr}$.

Fig. A6.5 **Plug flow and bubbly flow in a tilted evaporator.**

Figures A6.6 & A6.7 have been removed due to poor print quality

refer to page 53, $\phi_t = 30^\circ$, and $\phi_r = 0^\circ$;
 $\dot{q} = 20 \text{ kW/m}^2$, $\dot{m} = 0.91 \text{ kg/hr}$.

Fig. A6.6 The weak rivulet in a tilted condenser.

refer to Fig. 4.3 and page 53.
 $\dot{q} = 20 \text{ kW/m}^2$, $\dot{m} = 0.91 \text{ kg/hr}$.
 $\phi_t = 80^\circ$.

Fig. A6.7 Plug flow in the tilted evaporator.

Figures A6.8 has been removed due to poor print quality.

refer to page 54.
 $\dot{q} = 20 \text{ kW/m}^2$, $\dot{m} = 0.91 \text{ kg/hr}$.
 $\phi_t = 80^\circ$, $\phi_r = 0^\circ$.

Fig. A6.8 **Liquid slug pushed into condenser at the evaporator close to horizontal.**